INTERNATIONAL JOURNAL OF AUTOMOTIVE AND MECHANICAL ENGINEERING (IJAME)
ISSN: 2229-8649 e-ISSN: 2180-1606
VOL. 19, ISSUE 2, 9834 – 9858
DOI: https://doi.org/10.15282/ijame.19.2.2022.17.0759

ORIGINAL ARTICLE

Active Front Wheel Steering System using Yaw Rate Estimation based Fuzzy Logic Due to Various Lateral Wind Disturbance

T.L. Lok and V.R. Aparow*

Department of Electrical and Electronic Engineering, Faculty of Science and Engineering, University of Nottingham Malaysia Campus, Jalan Broga, 43500 Semenyih, Selangor Darul Ehsan, Malaysia

ABSTRACT – The paper devised and compared the performances of PID, fuzzy-tuned PID and fuzzy logic controller in an Active Front Wheel Steering system to stabilize a 9-DOF nonlinear passenger vehicle when subjected to lateral wind disturbance. The vehicle model was derived mathematically and verified with data from IPG CarMaker at a longitudinal speed of 80 km/h. Initially, the disturbance test was conducted using three lateral wind disturbance profiles to test for controller resiliency with zero steering input. Then, a simple but effective yaw rate observer was derived without compromising the linearity of the vehicle model to simulate the disturbance test with a double lane change (DLC) steering input. A more extreme disturbance magnitude was evaluated in the latter test using the developed control designs. The three controllers showed good performances in both disturbance tests, with fuzzy logic having the lowest error out of the three, which is less than 5% for using the estimated yaw rate observer.

ARTICLE HISTORY
Received: 29th June 2021
Revised: 12th June 2022
Accepted: 15th July 2022
Published: 5th Aug 2022

KEYWORDS
Active front wheel steering;
Fuzzy logic controller;
9DOF vehicle model;
Lateral wind disturbances;
IPG CarMaker

INTRODUCTION

Vehicle stability is a prominent area of research in automotive industries. This isn't surprising as humans had benefited immensely from the advent of vehicle be it for transportation or cargo shipping, and they would expect to operate the vehicle safely. The introduction of cruise control, anti-lock braking, and brake-force distribution system are some of the successes in vehicle stability research. Despite these control systems are deployed in the vehicle, there are other external disturbances that could jeopardize the lateral stability of the vehicle. These are the non-uniform road adhesion and side wind forces. The effect of side wind force on the vehicle depends on vehicle body contour, steering geometry, and vehicle mass, according to Diao et al. [2]. The latter two factors are usually constant for the vehicle, whereas the body contour can be amended to improve stability. However, an internal control system acting independently is preferred to control the vehicle's lateral stability as mechanical overhauls to the vehicle still require the driver's competency in dealing with wind disturbances. In order to control the lateral stability of the vehicle, yaw rate is used as the optimizing variable for stability assessment. This leads to the subject of controlling the yaw rate of the vehicle, whereby there are a few proposals made in automotive research namely using the four wheel steering system, active differential braking system, direct yaw moment control and active front wheel steering (AFWS) system [3]. However, AFWS is used as the main choice for controlling the yaw rate disturbance due to side wind force. The AFWS is designed by using an actuator motor to generate a corrective steering angle to minimize the unwanted disturbance in the lateral direction.

There are a lot of researchers have been conducted related to AFWS to minimize the lateral effect on the vehicle body due to unwanted lateral disturbances. It can be observed that Wu et al. [4] studied the robust vehicle yaw stability control by active front steering with an active disturbance rejection controller. The proposed algorithm can dynamically estimate and compensate for the total disturbance. Besides, the algorithm provides good control performance in a range of conditions using a simplified vehicle model. Similarly, Diao et al. [2] focused on the development of an active front wheel steering system using sideslip angle and sliding mode observer design to reject the unwanted side wind. The algorithm is verified using two degree of freedom integrate with a vehicle dynamic simulation tool called CarSim software. Futhermore, Zhao et al. [5] investigated the displacement and force coupling control design for an active front steering system. In this study, the research works emphasize more on developing robust yaw rate controller with H∞ for the nonlinear vehicle model to reject external disturbances due to road characteristics. Meanwhile, Saruchi et al. [6] studied Active Front Wheel Steering System using steer-by-wire to enhance vehicle handling performance without driver interference. The proposed control strategy is simulated using a simplified vehicle model in J-curve and Lane change manoeuvres with the presence of side wind disturbance using a simple PID controller. Additional, Hudha et al. [7] executed a Hardware-in-the-Loop simulation (HiLS) on a multi-DOF passenger vehicle model with AFWS using single input of side wind force as the lateral disturbances without implementation of rack and pinion steering model.

On the other hand, a lot of researches on myriad controllers have been investigated to control the AFWS using yaw rate as feedback loop control. Fuzzy logic can also be paired with a sliding mode controller (SMC) as presented by Ma et al. [8] for the cornering stability of AFWS vehicles. This study mainly emphasize on the approach using Takagi-Sugeno (T-S) fuzzy-based sliding mode control (SMC) strategy for the AFS system to improve the cornering stability of vehicles

*CORRESPONDING AUTHOR | V. R. Aparow | ✉ Vimal.Rau@nottingham.edu.my

only. A fancier approach was using neuro-fuzzy controller by Aalizadeh et al. [9], to which the controller performed better on the slippery road than conventional fuzzy logic. In this study, it was discovered that regardless of the friction coefficient, the neuro-fuzzy controller continuously tracked the desired yaw rate accurately for the AFWS whereas the PID controller deviated greater from the set point with decreasing friction coefficient. Moreover, Saikia et al. [10] studies on the generation of yaw moment and corrective steering angle for AFWS, which successfully tracked the yaw rate and sideslip angle with a correct trend using adaptive SMC. However, this study does not emphasize mainly on the disturbance rejection due to side wind forces.

Meanwhile, there is a lot of research using AFWS for disturbance rejection system due to gun recoil forces. It can be noted that Aparow et al. [11] developed several algorithms to reject unwanted disturbances due to gun recoil forces in lateral directions. The research works mainly used AFWS as the main aspect to improve armoured vehicle dynamic behaviors and added several additional active disturbance rejection algorithms. All the proposed algorithms are evaluated and the optimum algorithm is selected. Similarly, Mansor et al. [12] and Aparow et al. [13] developed a disturbance rejection control algorithm using AFWS for a wheeled armoured vehicle during firing conditions. The armoured vehicles are investigated at various speeds and various firing angles to evaluate the performance of the disturbance rejection control algorithm based on AFWS. Meanwhile, the researches on AFWS on armoured vehicles have been further investigated by Kadir et al. [14] and Aparow et al. [15], where the research works focused mainly from simulation-based testing to hardware-based testing using AFWS-based disturbance rejection control via yaw rate and lateral acceleration feedback loops. An armoured vehicle prototype based on the actual vehicle has been developed, and the proposed algorithm is implemented in the armoured vehicle for real-time testing. On the other hand, Aparow et al. [16] also implemented Artificial Neural Network as part of the AFWS-based estimated rejection algorithm to further enhance the previous algorithm in order to improve the dynamic performance of the armoured vehicle during firing. Based on the previous researches, it can be noted that the AFWS has been used mainly to enhance the lateral dynamics of vehicles during lateral disturbances due to side wind forces. However, shortcomings in previous works are the disturbance are considered as the constant and single inputs during the simulation testing. Other than that, a simplified vehicle model without considering the nonlinearity of the vehicle model and steering models are not mainly considered in the previous study. Moreover, extensive studies of AFWS using an estimated disturbance rejection algorithm are mainly implemented for armoured vehicle testing but not for passenger vehicles. Therefore, in this study, AFWS was developed using yaw rate estimation, and several controllers were used for the evaluation of the most optimum controller identified in this study.

In this paper, a nonlinear 9-DOF passenger vehicle is developed and verified using data from IPG CarMaker. This vehicle model is to be used together with the AFWS system in removing the yaw rate disturbance due to side wind force. Instead of just PID controller, fuzzy-tuned PID and fuzzy logic controller are developed, and together the performance of these three controllers will be compared in stabilizing the vehicle. Usually, the performance of the controllers is tested with a steering input of zero. However, this study will conduct an additional analysis which further verifies the controllers' performances with steering intervention, but this requires an observer that could give the desired yaw rate based on the steering input. According to studies done by Zhang et al. [17] and Li et al. [18], they used a 2-DOF linear vehicle model as a reference model to estimate the desired yaw rate for their research. Using a linear model will be less accurate than a nonlinear model. Consequently, part of the research in this paper will attempt to derive a yaw rate observer without reducing the linearity of the proposed vehicle model. This paper is organized as follows: Section 1 provides an introduction and background to the research in AFWS systems and its control system. It also explains the motivation for carrying out this research. Section 2 details the derivation of the 9-DOF passenger vehicle model, including the verification of the model with IPG CarMaker. Section 3 goes through the development of the control systems and yaw rate observer used in this study. Section 4 gives a run down on all the disturbance tests. It also contains all the results for each test, including their discussions. Section 5 is the final section which summarizes all the work done in this paper and makes a conclusion for the findings.

THE 9-DOF PASSENGER VEHICLE MODEL

The vehicle model is modelled using theories of vehicle dynamics and Newton's law of motions. It comprises several subsystems that describe the dynamics of different vehicle parts. These are the Pacejka Tire Model, Load Distribution Model, Handling Model, Rack and Pinion Steering Model, Lateral and Longitudinal Slip Model.

Modelling Assumptions

There are assumptions made in this study. Firstly, the vehicle is assumed always to be driving on a leveled road or non-inclined road. So, additional forces due to slope are ignored. Next, the coefficient of road friction is uniform throughout the road surface, which ensures any lateral disturbances are contributed only by the wind force. Besides, the vehicle model in this paper doesn't include the suspension or ride model; hence it only has 9-DOF instead of 14-DOF. Furthermore, the vehicle will always drive at a constant given speed without applying any braking torque in any test. Lastly, the vehicle is lumped into a single mass and the vehicle chassis is treated as a sprung mass.

Load Distribution Model

This subsystem shall estimate the vertical forces acting on each wheel as shown in Figures 1(a) and 1(b). Based on Aparow et al. [19], the vertical load can be modelled as a function of lateral and longitudinal acceleration, a_y and a_x. The assumptions made for the derivation of the formula are no suspension dynamics and the roll and pitch coupling are

neglected. The formula is based on the acceleration of vehicle chassis due to inertia. Through decoupling the roll and pitch dynamics, simple moment and static analysis would yield the vertical load equations, with attention given that M_v is the virtual mass, found using a simple relation below:

$$M_{v,i} = \frac{F_{z,i}}{g}, i = f\ (front) or\ r\ (rear) \tag{1}$$

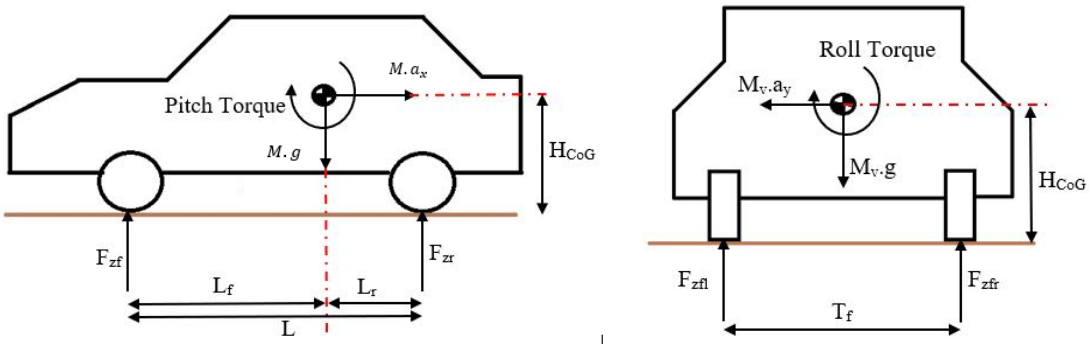

Figure 1. (a) Side view and (b) front or rear view of vehicle (front view in this case).

Despite ride model is not considered, this equation estimates the load to an accurate extend. The equations below show the vertical load equation for all four wheels.

$$F_{zfl} = M\left(\frac{L_r}{L}g - \frac{H_{CoG}}{L}a_x\right)\left(\frac{1}{2} - \frac{H_{CoG}a_y}{T_f g}\right) \tag{2}$$

$$F_{zfr} = M\left(\frac{L_r}{L}g - \frac{H_{CoG}}{L}a_x\right)\left(\frac{1}{2} + \frac{H_{CoG}a_y}{T_f g}\right) \tag{3}$$

$$F_{zrl} = M\left(\frac{L_f}{L}g + \frac{H_{CoG}}{L}a_x\right)\left(\frac{1}{2} - \frac{H_{CoG}a_y}{T_r g}\right) \tag{4}$$

$$F_{zrr} = M\left(\frac{L_f}{L}g + \frac{H_{CoG}}{L}a_x\right)\left(\frac{1}{2} + \frac{H_{CoG}a_y}{T_r g}\right) \tag{5}$$

where,

F_{zfl}, F_{zfr}	=	Vertical load on front left and right tyre (N)
F_{zrl}, F_{zrr}	=	Vertical load on rear left and right tyre (N)
M	=	Mass of the vehicle (kg)
H_{CoG}	=	Height of CoG of the vehicle from ground (m)
L_f	=	distance between front tyre axle and CoG (m)
L_r	=	distance between rear tyre axle and CoG (m)
T_f	=	Front track width (m)
T_r	=	Rear track width (m)
a_x	=	Longitudinal Acceleration (ms^{-2})
a_y	=	Lateral acceleration (ms^{-2})
L	=	Wheelbase (m)
g	=	Gravitational acceleration, 9.81 $kgms^{-2}$

Pacejka Tire Model

This is a crucial subsystem to estimate the aligning moment, lateral and longitudinal forces for each wheel, which is then used by the handling model to evaluate the accelerations and yaw moment. The Pacejka Tire Model or Magic Formula (MF) is chosen due to its accuracy in estimating the lateral and longitudinal dynamics. According to Ahmad et al. [20], the general force or moment equation is given below:

$$y(x) = D\sin\left(C\tan^{-1}\left(Bx - E(Bx - \tan^{-1}(Bx))\right)\right) \tag{6}$$

$$Y(X) = y(x) + S_v \tag{7}$$

$$x = X + S_h \tag{8}$$

Where,

B	=	Stiffness factor
C	=	Shape factor
D	=	Peak value

E = Curvature factor
S_v = Vertical shift
S_h = Horizontal shift

For lateral force and aligning moment, X denotes the slip angle, α whereas for longitudinal force or brake force, X denotes the longitudinal slip, κ. Magic Formula is a semi-empirical tire model. It is formulated based on experimental attempts with slight theory. The finalized equation was decided based on the similarity method, which is how well the equation fits the experimental data. Depending on the different coefficients that made up these six factors, the longitudinal tire force, lateral tire force and the tire moment can be obtained, in which they are represented as a general function, $y(x)$. $Y(X)$ is attained when the vertical shift is factored in. Detail explanation can be obtained from Aparow et al. [19] and Ahmad et al. [20].

Handling Model

This section presents the 7-DOF nonlinear vehicle model. Three degrees of freedom represent the lateral, longitudinal and yaw motion. Another one degree of freedom represents the rolling motion of each wheel of the vehicle. Hence, four wheels make up to the remaining four degrees of freedom. The wheel motion is covered in the next subsection. This allows both decoupled roll and pitch torque to be present for derivation of the load distribution model. For acceleration, longitudinal acceleration and velocity of the vehicle are represented as a_x and V_x, whereas lateral acceleration and velocity of the vehicle are represented as a_y and V_y. Figure 2 shows the vehicle model diagram.

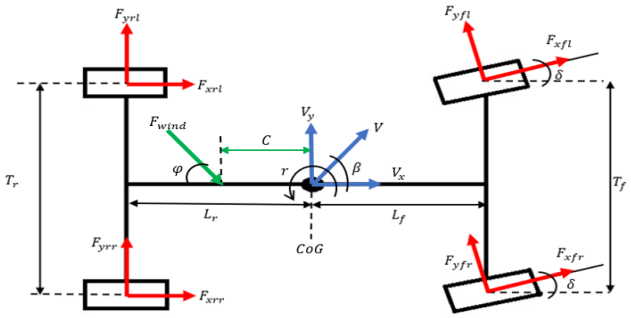

Figure 2. 7-DOF vehicle handling model.

Acceleration in the lateral direction or y-axis is given as:

$$\dot{V_y} = a_x + \dot{r}.V_y \tag{9}$$

And a_x can be calculated by summing all forces in the longitudinal direction.

$$a_x = \frac{[F_{tractive} + F_{aero} + F_{resist} + F_{wind}\cos\varphi]}{M} \tag{10}$$

The total tractive force, $F_{tractive}$ is given below as,

$$F_{tractive} = F_{xrl} + F_{xrr} + (F_{xfl} + F_{xfr})\cos\delta + (F_{yfl} + F_{yfr})\sin\delta \tag{11}$$

The aerodynamic drag force, F_{aero} is given as,

$$F_{aero} = \frac{1}{2}\rho C_d A {V_x}^2 \tag{12}$$

The resistive force due to rolling resistance, F_{resist} is given as,

$$F_{resist} = MC_r gV_x \tag{13}$$

Acceleration in the longitudinal direction or x-axis is given as,

$$\dot{V_x} = a_y - \dot{r}.V_x \tag{14}$$

And a_y can be calculated by summing all forces in the lateral direction.

$$a_y = \frac{[F_{yrl} + F_{yrr} + (F_{yfl} + F_{yfr})\cos\delta - (F_{xfl} + F_{xfr})\sin\delta + F_{wind}sin\ \varphi]}{M} \tag{15}$$

where,

$F_{xfl}, F_{xfr}, F_{xrl}, F_{xrr}$ = Longitudinal force for front and rear wheel (N)
$F_{yfl}, F_{yfr}, F_{yrl}, F_{yrr}$ = Lateral force for front and rear wheel (N)
$\dot{r}$ = Yaw rate (Rads^{-1})
δ = Wheel steering angle (Rad)
V_x = Longitudinal velocity (ms^{-1})
V_y = Lateral velocity (ms^{-1})
ρ = Air density = 1.206 (kgm^{-3})
C_d = Aerodynamic drag coefficient = 0.19
C_r = Rolling resistance coefficient = 0.014 (m^{-1})
A = Frontal area of vehicle (m^2)
F_{wind} = Wind force (N)
φ = angle of wind force (rad)
C = distance between the wind's center of pressure (CoP) and CoG (m)

The yaw acceleration, $\ddot{r}$ is evaluated by equating the sum of moment referencing to the centre of gravity to zero.

$$\ddot{r} = \frac{\begin{bmatrix} -L_r(F_{yrl}+F_{yrr}) + L_f\left((F_{yfl}+F_{yfr})\cos\delta - (F_{xfl}+F_{xfr})\sin\delta\right) \\ +\frac{T_r}{2}(F_{xrl}-F_{xrr}) + \frac{T_f}{2}\left((F_{yfl}-F_{yfr})\sin\delta + (F_{xfl}-F_{xfr})\cos\delta\right) \\ +M_{align} + C.F_{wind}\sin\varphi \end{bmatrix}}{I_z} \tag{16}$$

I_z is the moment of inertia of the vehicle about the z-axis. M_{align} is the sum of aligning moment, M_z for each wheel obtain from the tire model. C is a signed value, in which it is positive when wind force is acting to the right of the center of gravity and it is negative when wind force is acting to the left of the center of gravity.

$$M_{align} = M_{zfl} + M_{zfr} + M_{zrl} + M_{zrr} \tag{17}$$

Vehicle lateral slip angle model

The values of V_x and V_y are attained by integrating $\dot{V_x}$ and $\dot{V_y}$. These values are important to derive the tire slip angle formula.

$$\alpha_{fl} = \tan^{-1}\left(\frac{V_y + L_f.\dot{r}}{V_x - T_f.\frac{\dot{r}}{2}}\right) - \delta \tag{18}$$

$$\alpha_{fr} = \tan^{-1}\left(\frac{V_y + L_f.\dot{r}}{V_x + T_f.\frac{\dot{r}}{2}}\right) - \delta \tag{19}$$

$$\alpha_{rl} = \tan^{-1}\left(\frac{V_y - L_r.\dot{r}}{V_x - T_r.\frac{\dot{r}}{2}}\right) \tag{20}$$

$$\alpha_{rr} = \tan^{-1}\left(\frac{V_y - L_r.\dot{r}}{V_x + T_r.\frac{\dot{r}}{2}}\right) \tag{21}$$

Where,

$\alpha_{fl}, \alpha_{fr}, \alpha_{rl}, \alpha_{rr}$ = Slip angle for front and rear wheel (rad)

The sideslip angle of the vehicle, β is evaluated as below:

$$\beta = \tan^{-1}\left(\frac{V_y}{V_x}\right) \tag{22}$$

Vehicle Longitudinal Slip Model

The longitudinal slip of the vehicle can also be evaluated but first it is required to determine the longitudinal velocity component of the front and rear wheels. The velocity of the front wheel is given below:

$$V_f = \sqrt{\left(V_y + L_f.\dot{r}\right)^2 + {V_x}^2} \tag{23}$$

Hence, the longitudinal velocity component of the front wheel is given below:

$$V_{xf} = V_f \cos \alpha_f \tag{24}$$

The velocity of the rear wheel is given below:

$$V_r = \sqrt{\left(V_y + L_r.\dot{r}\right)^2 + {V_x}^2} \tag{25}$$

Hence, the longitudinal velocity component of the rear wheel is given below:

$$V_{xr} = V_r \cos \alpha_r \tag{26}$$

The longitudinal slip of the front and rear wheel are given below:

$$\kappa_{f,r} = \frac{V_{xf,r} - \omega_{f,r}.R}{V_{xf,r}} \tag{27}$$

Where,

ω_f , ω_r = Angular velocity front and rear wheels (rads^{-1})
R = Radius of front and rear wheels (m)

Wheel Dynamic Model

There are throttling and braking torque acting on the wheel. The viscous force also exerts torque onto the wheel. Figure 3 shows the free body diagram of a vehicle wheel.

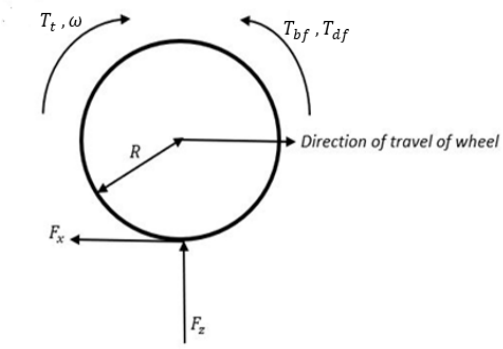

Figure 3. Free body diagram of wheel.

The resultant torque on the wheel can be expressed in terms of angular acceleration, as shown below:

$$I_{wheel}.\dot{\omega} = F_x.R - T_{bf} + T_t - T_{df} \tag{28}$$

Where,

I_{wheel} = moment of inertia of wheel about axis of revolution (kgm^2)
$\dot{\omega}$ = Angular acceleration of wheel (rads^{-2})
T_{bf} = Braking Torque (Nm)
T_t = Throttling torque (Nm)
T_{df} = torque due to Viscous force (Nm)

In order to find the angular velocity of each wheel, equate the longitudinal force of the chosen wheel as F_x, then solve Eq. (28) to obtain the angular acceleration. Finally, the value ω is from the integration of angular acceleration. The value of T_{bf} = 0 whereas T_{df} is represented as $T_{df} = \mu\omega$.

2-DOF Rack and Pinion Steering Model

The rack and pinion steering system is suitable for passenger vehicles due to their simple construction and compactness. In order to support the concept of the AFWS system, the steering model used in this project would be a 2-DOF system modelled after the column-type electric power-assisted steering (EPAS). Column-type EPAS is chosen as it can be easily installed into the vehicle. One degree of freedom is for the steering column while the remaining goes to the steering rack, as explained in Ramesh et al. [22] and Aparow et al. [21]. Figure 4 shows the complete layout of a rack and pinion steering system. The power assist unit including the electric motor is installed at the steering column for column-type EPAS. To derive a simplified steering model, a few assumptions are made. It is assumed all mechanical connections are rigid. Next, the mass of tie rods and tires are neglected. Furthermore, the EPAS system are made up by three basic elements, which are the steering column, steering linkage, and DC motor. All elements behave as a spring and damper system.

DC motor model:

The DC motor is modelled with electrical and mechanical components. Using Kirchhoff Voltage Law (KVL) on the motor circuit in Figure 5, the DC input voltage to the DC motor is evaluated as:

$$e_m = R_a.I_a + L_a.\dot{I_a}.N_1 + e_b \tag{29}$$

And the electromotive force of the DC motor is given as:

$$e_b = K_b.\dot{\theta}_{sc}.N_1 \tag{30}$$

The motor torque is then formulated as below:

$$T_{mech} = K_t.I_a.N_1 \tag{31}$$

Where,

e_m = DC input voltage (V)
e_b = Electromotive force (V)
R_a = Armature winding resistance, taken as (Ω)
I_a = Armature current (A)
L_a = Armature winding inductance (H)
N_1 = DC motor gear ratio
K_b = Electromotive force constant ($V/rads^{-1}$)
K_t = motor torque constant (Nm/A)
T_{mech} = DC motor torque (kgm^2s^{-2})
θ_{sc} = Angular displacement of steering column (rad)

Substituting Eq. (29) into Eq. (31), the resulting motor torque is given below.

$$T_{mech} = \frac{K_t.N_1}{R_a}\left[e_m - \left(K_b.\dot{\theta}_{sc}.N_1\right) + \left(L_a.\dot{I_a}.N_1\right)\right] \tag{32}$$

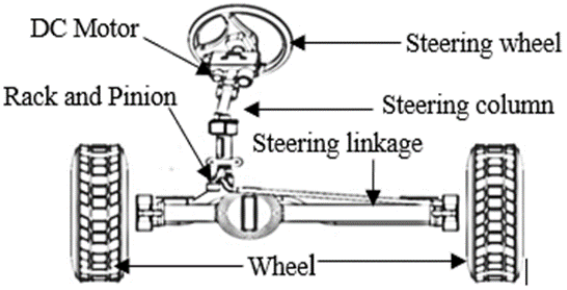

Figure 4. General rack and pinion steering system.

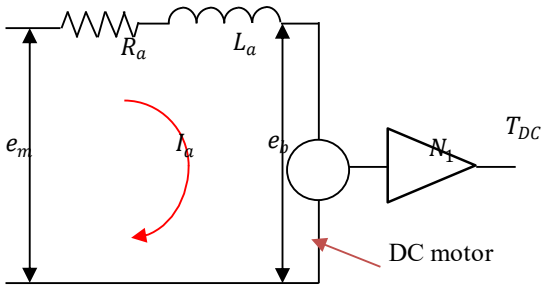

Figure 5. Circuit model of the DC motor.

Steering column equation:

The resultant torque on the steering column can be modelled by considering the viscous damping, rotational stiffness and moment of inertia of the steering column, given by Ramesh et al. [22].

$$J_{eq}.\ddot{\theta}_{sc} + B_{eq}.\dot{\theta}_{sc} + K_{sc}.(\theta_{sc} - \theta_{sw}) = T_{mech} - T_{pinion} \tag{33}$$

Meanwhile, the equivalent moment of inertia and viscous damping are given as:

$$J_{eq} = J_{sc} + \left({N_1}^2.J_m\right) \tag{34}$$

$$B_{eq} = B_{sc} + (N_1.B_m) \tag{35}$$

Where,

J_{sc} = moment of inertia of steering column (kgm^2)
J_m = moment of inertia of DC motor (kgm^2)
θ_{sc} = Angular displacement of steering column (rad)
K_{sc} = Rotational stiffness of steering column (Nm/rad)
θ_{sw} = Angular displacement of steering wheel (rad)
N_1 = DC motor gear ratio
B_{sc} = Viscous damping of steering column (Nm/rads^{-1})
B_m = Viscous damping of DC motor (Nm/rads^{-1})
T_{pinion} = torque due to pinion linkage (Nm)

Steering linkage equation:

The translational motion of the rack due to the rotation of the pinion is related to the equation below.

$$M_r.\ddot{y_r} + B_r.\dot{y_r} + CF_R.sgn(\dot{y_r}) = \eta_F \frac{T_{pinion}}{R_{pinion}} + \eta_B \frac{T_{kl}}{N_L} \tag{36}$$

And the pinion torque is given below.

$$T_{pinion} = K_{tr}.\left(\theta_{sc} - \frac{y_r}{R_{pinion}}\right) \tag{37}$$

Where,

M_r = Mass of rack (kg)
R_{pinion} = Radius of pinion (m)
CF_R = Coulomb friction breakout force on steering rack (N)
B_r = Viscous damping of steering column (Nm/rads^{-1})
y_r = displacement of steering rack (m)
N_L = Gear ratio efficiency of steering linkage
η_F = Gear ratio efficiency of forward transmission
η_B = Gear ratio efficiency of backward transmission
K_{tr} = Tie rod rotational stiffness (Nm/rad)
T_{kl} = torque at steering linkage (Nm)
θ_{sc} = Angular displacement of steering column (rad)
T_{pinion} = torque due to pinion (Nm)

Road wheel equation

Till this point, the translational motion of the rack has been defined. To complete the steering model, this rack motion must be converted to the angular motion of the rolling wheels to be used with the handling model. For front wheel steering, this is made possible with the equation below, according to Ramesh et al. [22]. Figure 6 shows the complete block diagram of the rack and pinion steering model.

$$J_{fw}.\ddot{\delta} + B_{fw}.\dot{\delta} + CF_{fw}.sgn(\dot{\delta}) = T_{kl} + T_{ext} \tag{38}$$

And the torque exerted on the steering linkage,

$$T_{kl} = K_{sl}.\left(\frac{y_r}{N_L} - \delta\right) \tag{39}$$

Where,

J_{fw} = moment of inertia of front wheel (kgm^2)
δ = Angular displacement of front wheel (rad)
CF_{fw} = Coulomb friction breakout force on front wheel (N)
B_{fw} = Viscous damping of front wheel (Nm/rads^{-1})
y_r = displacement of steering rack (m)
N_L = Gear ratio efficiency of steering linkage
K_{sl} = Rotational stiffness due to steering linkage (Nm/rad)
T_{kl} = torque at steering linkage (Nm)
T_{ext} = External torque on road wheel (Nm)

Based on the rack and pinion steering system, the complete passenger vehicle model block diagram is shown in Figure 7. In this block diagram, the main input focuses on the steering input to control the lateral motion of the passenger vehicle, whereby the braking input is considered zero and throttle input is considered as constant engine torque for the passenger vehicle.

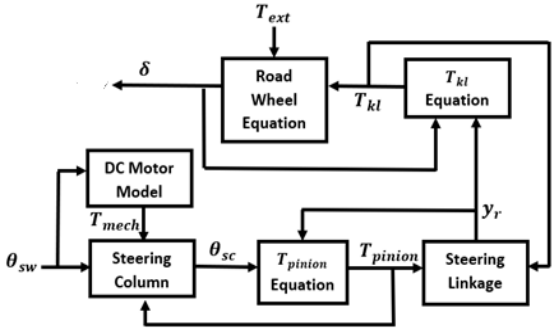

Figure 6. 2-DOF rack and pinion steering model.

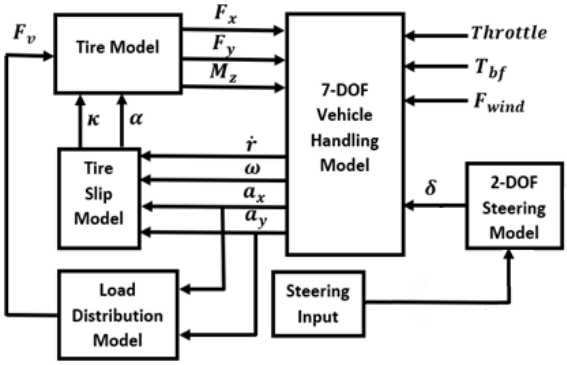

Figure 7. A 9-DOF passenger vehicle model.

VERIFICATION OF PASSENGER VEHICLE MODEL USING IPG CARMAKER

With all the important vehicle subsystems derived, the passenger vehicle developed using Matlalb Simulink can be verified using data from IPG CarMaker, a vehicle dynamic simulation software. It can be noted from Aparow et al. [38], the verification method is referred to as the similarity identification of the vehicle behaviour, and the response does not

concern perfect fitting with the actual system. This is mainly because the verification process is conducted to obtain a confident level of the model accuracy before proceed with controller development. The verification test is done using different testing scenarios based on the Society of Automotive (SAE) standard, such as Double Lane Change (DLC) and Slalom at a vehicle speed of 80 km/h. By inputting a steering input into the vehicle model, the waveform of the output, mainly the lateral dynamics as lateral stability is the interest in this study, will be compared with that from IPG CarMaker. These outputs are the lateral acceleration, yaw rate and the body sideslip angle. The vehicle parameters are based on the Beetle Volkswagen vehicle model from IPG CarMaker. Table 1 shows the specifications of the Beetle vehicle model, whereas Table 2 shows the values of all constants used in the rack and pinion steering model. In IPG CarMaker, Scenario Editor was used to develop the road model to design the testing procedure for three different based on SAE standards. All the testing procedure using IPG CarMaker is shown in Figure 8(a) and 8(b). Meanwhile, all the results between Matlab Simulink based vehicle model and IPG CarMaker vehicle model are verified before proceeding with the development of Active Front Wheel Steering system.

Table 1. Vehicle model specifications.

Specifications	Abbreviation	Value	Unit
Mass of vehicle	M	1274	kg
Moment of inertia about z-axis	I_Z	1523	kgm^2
Wheelbase	L	2.578	m
Distance between front wheel axle to CoG	L_f	1.016	m
Distance between rear wheel axle to CoG	L_r	1.562	m
Height of CoG	H_{CoG}	0.540	m
Front track width	T_f	1.539	m
Rear track width	T_r	1.539	m
Wheel radius (free rolling)	R	0.316	m
Moment of inertia for wheel	I_{wheel}	0.615	kgm^2
Frontal area	A	1.6	m^2

Table 2. All constants and their values for the steering model.

Specifications	Abbreviation	Value	Unit
Mass of rack	M_r	15	kg
Viscous damping of rack	B_r	88.128	Nm/(rads^{-1})
Viscous damping of steering column	B_{sc}	0.360	Nm/(rads^{-1})
Viscous damping of front wheel	B_{fw}	88.128	Nm/(rads^{-1})
Viscous damping of motor	B_m	0.05	Nm/(rads^{-1})
Moment of inertia of steering column	J_{sc}	0.0344	kgm^2
Moment of inertia of front wheel	J_{fw}	0.615	kgm^2
Moment of inertia of motor	J_m	0.00035	kgm^2
Rotational stiffness of steering column	K_{sc}	42057	Nm/rad
Rotational stiffness of steering linkage	K_{sl}	42057	Nm/rad
Rotational stiffness of tie rod	K_{tr}	42057	Nm/rad
Coulomb friction breakout force on rack	CF_r	0.04	N
Coulomb friction breakout force on road wheel	CF_{fw}	0.04	N
Armature inductance	L_a	0.0001	H
Armature resistance	R_a	0.1	Ω
Electromotive force constant	K_b	0.0533	V/(rads^{-1})
Motor torque constant	K_t	0.0533	Nm/A
Motor gear ratio	N_1	16:3	-
Steering linkage rate	N_L	0.118	m
Radius of pinion	R_{pinion}	0.00737	m
Gear efficiency for forward transmission	η_F	0.985	-
Gear efficiency for backward transmission	η_B	0.985	-
External torque on road wheel	T_{ext}	0	Nm

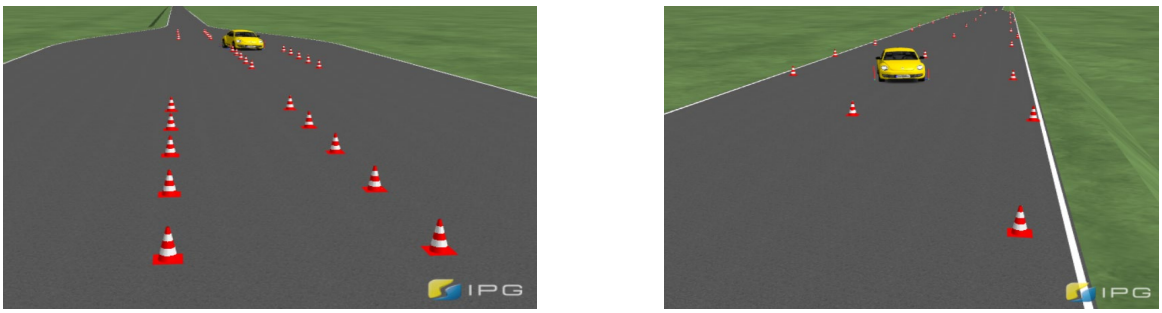

(a) (b)

Figure 8. (a) Double lane change test and (b) slalom test at 80 km/h.

Double Lane Change Verification Results

In this testing procedure, the vehicle speed is increased from 0 km/h to 80 km/h and the testing was conducted using a road model created using the Scenario Editor. Once the vehicle reached to optimum vehicle speed of 80 km/h, a double lane change steering input angle was applied to the vehicle model, as shown in Figure 9. Based on the steering input at travelling constant speed of 80 km/h, the lateral performance of the passenger vehicle is obtained from IPG Control such as yaw rate, lateral acceleration and body sideslip angle. The responses are compared with the vehicle simulation model as shown in Figure 10(a) to 10(c). From the verification results, it can be observed that the 9 DOF passenger vehicle model is able to follow the lateral responses from IPG CarMaker. The percentage of root mean square (RMS) error for the yaw rate response is 4.6%, lateral acceleration response is 3.86%, and body sideslip angle response is 8.7%, where the errors are less than 15%. The small deviation in magnitude occurred in the verification results since the data used in IPG CarMaker are developed by considering additional environmental effects such as road geometry, coefficients of friction, wind.

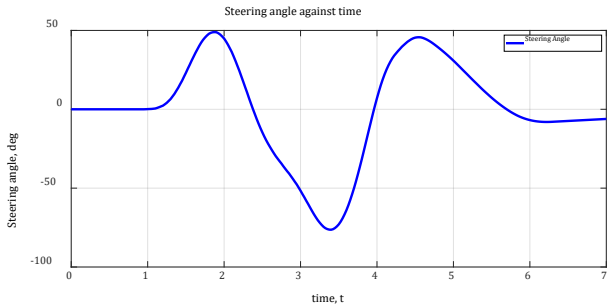

Figure 9. Steering angle input for verification procedure.

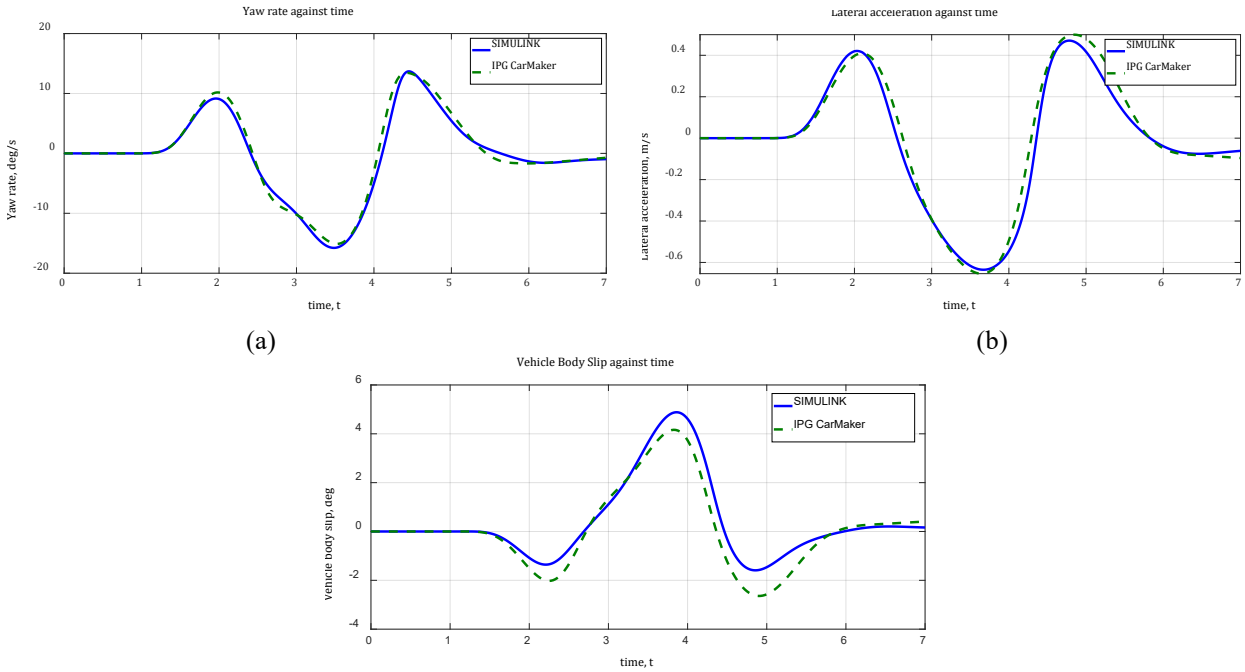

(a) (b)

Figure 10. Comparison of (a) yaw rate, (b) lateral acceleration and (c) body sideslip angle responses.

Slalom Verification Results

The test results of the slalom test at 80 km/h indicated that the simulation responses and vehicle model from IPG CarMaker were relatively in good agreement, as shown in Figure 12(a) to 12(c). Figure 11 shows the steering wheel input from IPG CarMaker which is used as the input for the simulation model during slalom test.

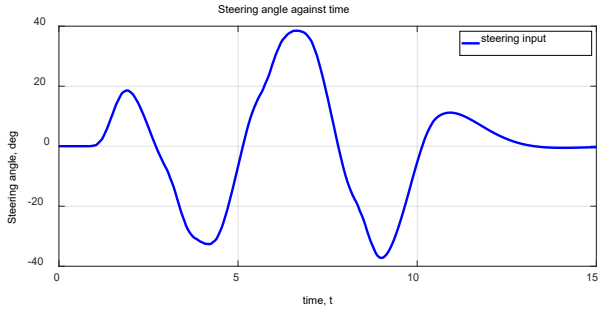

Figure 11. Steering angle input for verification procedure.

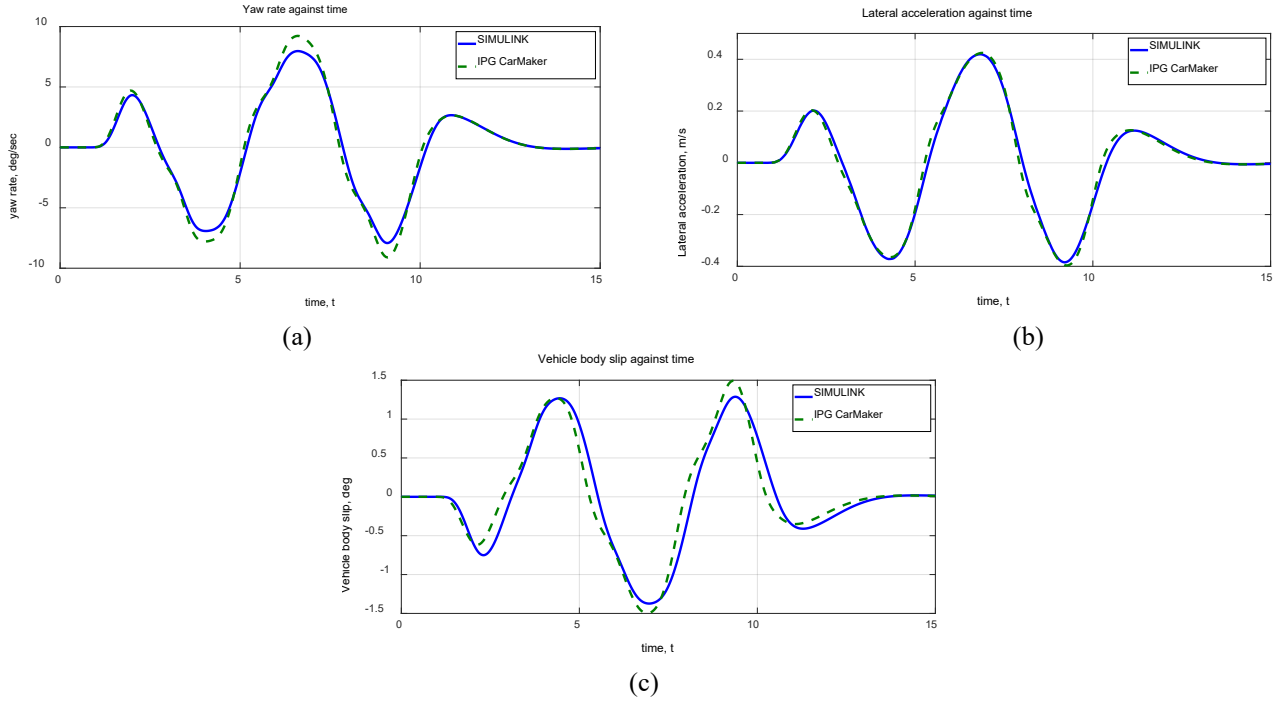

Figure 12. Comparison of (a) yaw rate, (b) lateral acceleration and (c) body sideslip angle responses.

In terms of yaw rate, lateral acceleration and body slip angle, it can be seen clearly that the simulation model results able to follow the IPG CarMaker data with minor deviation in trend and also the magnitude as described in Figure 12(b), 12(c) and 12(d). The percentage of RMS error for the Slalom test is 3.7% for yaw rate response, 4.1% for lateral acceleration and 4.6% for body sideslip angle. The minor deviation occurred in most of the simulation results due to high flexibility in the IPG CarMaker software which is considered ride model. However, the overall performance of the 9 DOF passenger vehicle is able to follow the behavior of the vehicle model from IPG CarMaker.

CONTROL SYSTEM AND OBSERVER MODELLING

This section focuses on the modelling and development of PID, Fuzzy-tuned PID and Fuzzy Logic controller scheme for AFWS system integrated in a closed loop model of the 9-DOF passenger vehicle model. It also explains the derivation of the yaw rate observer for used in the second disturbance test with nonzero steering input. All disturbance tests and analysis of their results will be discussed in the next section.

Control Design 1: PID Controller

Based on SIMULINK's PID block diagram, the equation used is given below:

$$G_{PID}(s) = K_p + K_i \frac{1}{s} + K_d \left(\frac{N}{1 + \frac{N}{s}} \right) \tag{40}$$

Where,

K_p = Proportional gain
K_i = Integral gain
K_d = Derivative gain
N = Noise coefficient

K_p, K_i and K_d are tuning parameters while N is kept at a low value, in this case, 10. By keeping N low, it will reduce the effect of a purely derivative term in the controller equation; hence high frequency noises will not be greatly amplified due to the strong derivative term. The control strategy is to use the yaw rate error as the input to the controller to output the corrected steering angle as input to the rack and pinion steering model.

$$e_{\dot{r}} = \dot{r}_{desired} - \dot{r}_{actual} \tag{41}$$

$$\delta_{corrected} = G_{PID}(s).e_{\dot{r}} \tag{42}$$

The closed-loop model is made with the negative feedback path of the actual yaw rate output by the vehicle handling model. For an optimum controller performance for all wind disturbance profiles, the final gain parameters are tuned with $K_p = 100$, $K_i = 0.05$ and $K_d = 25$. These gain parameters are used for all disturbance tests with or without steering input. Figure 19 shows the closed-loop model of the vehicle system with PID controller:

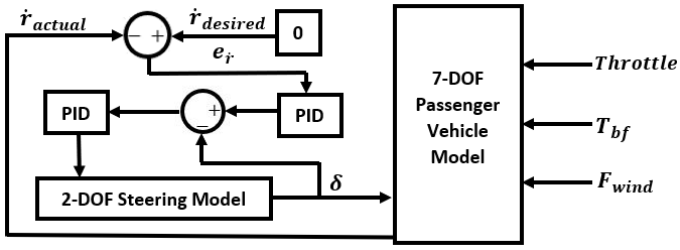

Figure 13. Closed loop model with PID.

Control Design 2: Fuzzy-tuned PID Controller Design

Using MATLAB's Fuzzy Logic Designer App, the nonlinear controller can be derived easily. The idea behind the fuzzy-tuned PID controller is the tuning gain parameters are not constant and are subject to change according to the inputs to the fuzzy logic controller. In other words, the fuzzy logic controller is used to tune the gains of the PID from time to time to ensure the PID controller can cope with myriad disturbance profiles. For this control scheme, the Mamdani Fuzzy Inference System (FIS) model is used with the centroid method and ANDing-type aggregation rule for defuzzification. Two inputs are used, which are the error and its derivative, the error rate. Error is calculated using Eq. (41). Both inputs' membership functions are shown in Figure 14.

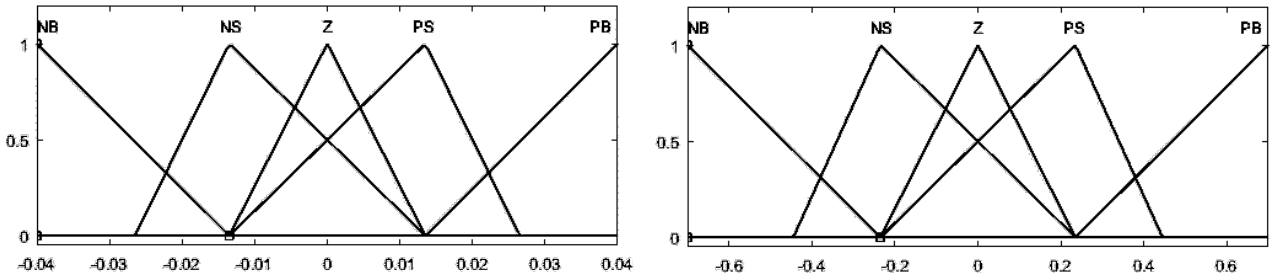

(i) error (ii) error rate

Figure 14. (i) Error and (ii) error rate membership function for Fuzzy-tuned PID.

The output of the Fuzzy-tuned PID controller is none other than K_p, K_i and K_d. Once again, the noise coefficient, N is kept at 10 as a constant. Hence, there are three output membership functions for each PID gain, as shown in Figure 15.

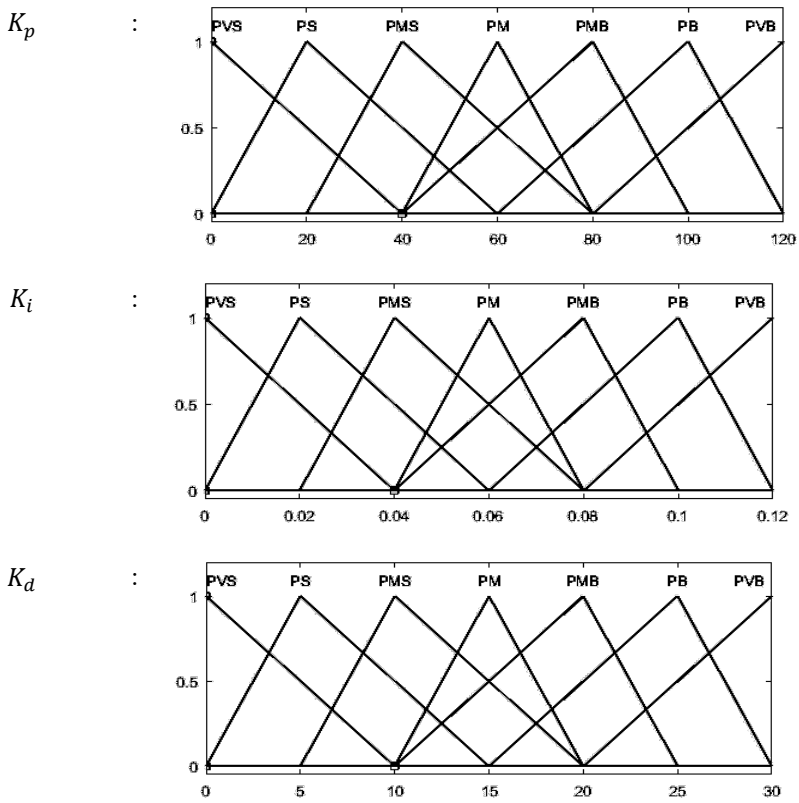

Figure 15. K_p, K_i and K_d membership function for Fuzzy-tuned PID.

Table 4, Table 5, and Table 6 show the 25 IF-THEN fuzzy rules for output K_p, K_i and K_d within their lookup table. The labels used for the membership functions are defined in Table 3:

Table 3. Meaning of the labels used for membership functions for fuzzy-tuned PID.

Labels	Meaning
NB	Negative Big
NS	Negative Small
Z	Zero
PVS	Positive Very Small
PS	Positive Small
PMS	Positive Medium Small
PMB	Positive Medium Big
PB	Positive Big
PVB	Positive Very Big

Table 4. Fuzzy Lookup Table for proportional gain in Fuzzy-tuned PID.

de/dt \ e	NB	NS	Z	PS	PB
NB	PVB	PVB	PVB	PVB	PVB
NS	PMB	PMB	PMB	PB	PVB
Z	PVS	PVS	PS	PMS	PMS
PS	PMB	PMB	PMB	PB	PVB
PB	PVB	PVB	PVB	PVB	PVB

Table 5. Fuzzy Lookup Table for integral gain in Fuzzy-tuned PID.

de/dt \ e	NB	NS	Z	PS	PB
NB	PM	PM	PM	PM	PM
NS	PMS	PMS	PMS	PMS	PMS
Z	PS	PS	PVS	PS	PS
PS	PMS	PMS	PMS	PMS	PMS
PB	PM	PM	PM	PM	PM

Table 6. Fuzzy Lookup Table for derivative gain in Fuzzy-tuned PID.

de/dt \ e	NB	NS	Z	PS	PB
NB	PVS	PMS	PM	PB	PVB
NS	PMS	PMB	PB	PVB	PVB
Z	PM	PB	PB	PVB	PVB
PS	PMS	PVB	PVB	PVB	PVB
PB	PVB	PVB	PVB	PVB	PVB

Example of Fuzzy rule:

$$IF\ (e = PB)\ AND\ (\dot{e} = PB), THEN\ (K_p = PVB), (K_i = PM)\ AND\ (K_d = PVB)$$

The fuzzy rule works this way; take K_p gain output as an example. If error and error rate falls in PB, this means there is a large deviation between the actual and desired yaw rate. To correct it, K_p value must be large; hence its value falls under PVB, as shown in Table 4. Figure 16 shows the layout of the Fuzzy-tuned PID controller with the nonlinear vehicle model in a closed loop system.

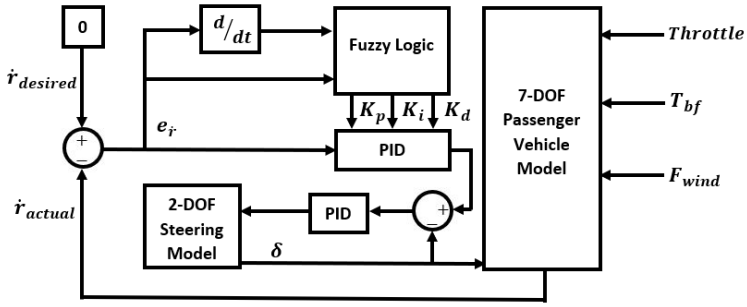

Figure 16. Closed loop model with fuzzy-tuned PID.

Control Design 3: Fuzzy Logic Controller Design

This fuzzy logic controller is also based on the Mamdani model with a centroid method and ANDing-type aggregation for defuzzification. However, the input and output membership functions and their range of values are completely different from the fuzzy-tuned PID below explains why:

i. The output of the fuzzy logic controller is the correction angle to be superposed to the steering input. On the other hand, the Fuzzy-tuned PID outputs the tuned gain parameters for PID.

ii. Fuzzy-tuned PID is predominantly a PID controller but more adaptive. Hence, the range of input and output membership function values are chosen with reference to the values of error, error rate and corrected steering input when the PID controller is used alone.

Like fuzzy-tuned PID, two inputs are used, which are the error and error rate. Figure 17 shows the input membership function for this controller. Meanwhile, Figure 18 shows the single output fuzzy logic controller membership function.

Error (range value $\times 10^{-3}$) :

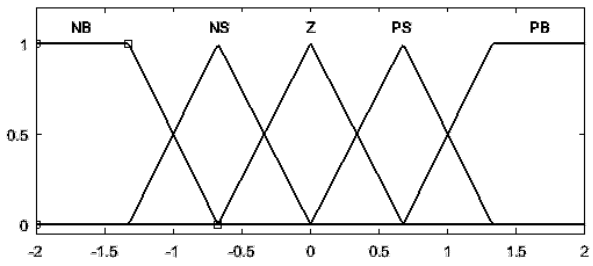

Error Rate :

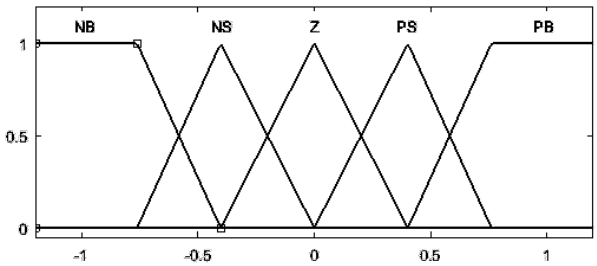

Figure 17. Error and error rate membership function for fuzzy logic controller.

Correction Angle :

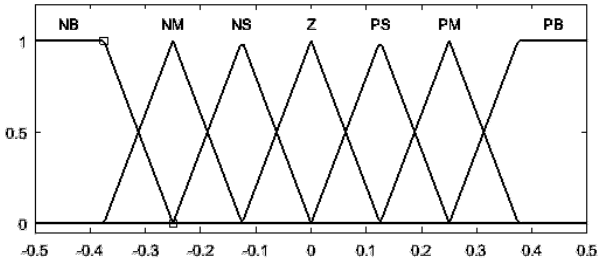

Figure 18. Correction angle membership function for fuzzy logic controller.

Table 8 shows the 25 IF-THEN fuzzy rules within the lookup table for correction angle. Table 7 shows the meaning of each label used for the membership function. Example of fuzzy rule:

$$IF\ (e = PB)\ and\ (\dot{e} = PB), THEN\ (\delta_{correction} = PB)$$

The fuzzy rule for this case works similarly to that for Fuzzy-tuned PID. When error and error rate values fall in PB, the wheel didn't steer as much as it should according to the steering input in the positive direction; hence large positive correction angle is needed to be added to the steering input via electric motor. This large correction angle has a value that falls under PB, shown in Table 8. The correction angle is superposed with the steering input as shown in Eq. (43), resulting in the corrected steering input, which will be fed into the steering model. Meanwhile, Figure 19 shows the fuzzy logic controller with the vehicle model in a closed loop system:

$$\delta_{corrected} = \delta_{input} + \delta_{correction} \tag{43}$$

Table 7. Meaning of labels of membership function for fuzzy logic controller.

Labels	Meaning
NB	Negative Big
NM	Negative Medium
NS	Negative Small
Z	Zero
PS	Positive Small
PM	Positive Medium
PB	Positive Big

Table 8. Fuzzy Lookup Table for correction angle in fuzzy logic controller.

de/dt \ e	NB	NS	Z	PS	PB
NB	NB	NM	NM	NS	Z
NS	NM	NM	NS	Z	PS
Z	NB	NS	Z	PS	PB
PS	NS	Z	PS	PM	PM
PB	Z	PS	PM	PM	PB

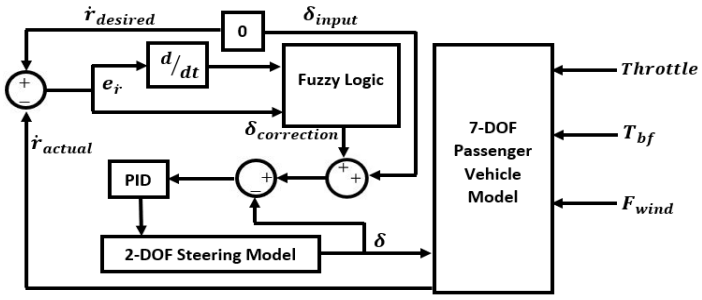

Figure 19. Closed loop model with fuzzy logic controller.

Control Design 4: Estimated Yaw Rate Observer using Control Design (1), (2) and (3)

This observer aims to estimate the desired yaw rate given a steering input, to allow the negative feedback error of the closed-loop vehicle model to be calculated, which in turn, the error is used by the controllers to reject unwanted disturbance and track the desired lateral dynamics more accurately at nonzero steering input. There are myriad ways to design a yaw rate observer, where the two prominent approaches to the observer design besides using a reference model are either:

i. Using a Kalman Filter and its variants, such as Extended Kalman Filter or Unscented Kalman Filter.
ii. Using a simple linear yaw rate to steering gain ratio.

However, the latter is not possible as the ratio is derived from a linear vehicle model, whereas using a Kalman Filter requires linearizing the nonlinear 9-DOF vehicle model to derive the state-space model. If possible, the yaw rate observer should be designed without compromising the complexity of the vehicle model. Hence, another simple but feasible and less mathematically intense approach is to find a ratio between yaw rate and steering input. Unlike the linear yaw rate to steering gain ratio, this method uses the actual yaw rate outputted by the SIMULINK 9-DOF vehicle model and mapped it onto the steering input. Since the vehicle model produces the correct output waveform given the DLC steering input in the verification test, the same steering input for the verification test at 120 km/h and its corresponding yaw rate output will be used to derive the observer, as illustrated in Figure 20(a). To ensure this method of constructing the observer is acceptable, the observer will also be derived at speed of 40 km/h using the same steering input as 120 km/h. With that, the performance of the observer can be evaluated using both of these speeds. With this method, the ratios calculated at different speed will be different since the yaw rate has different magnitude at different speed, as depicted in Figure 20(b).

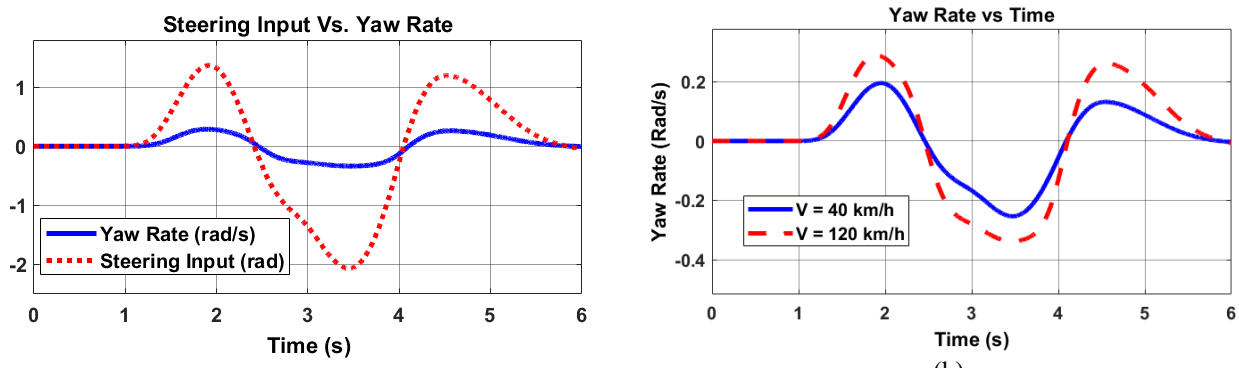

(a) (b)

Figure 20. Comparison of (a) yaw rate output at different speeds and (b) steering input and its yaw rate.

To derive the observer, the yaw rate to steering input ratio is first calculated across the waveform, and then the mean ratio is obtained from that array of ratios because the value of the ratios across the waveform will never be equal. However, a direct division of yaw rate by the steering input using their whole data array is impossible as the mean ratio will be skewed by very large or very small ratio values when either the yaw rate or steering input or both have very infinitesimal value. This issue is also contributed by a slight time shift between the steering input and the yaw rate plots, which is less obvious but detectable in Figure 20(a).

To rectify the problem of the mean being susceptible to unwanted outliers, the ratios are calculated across the data array of steering input and yaw rate between a time window of 1.2s to 2.2s, 2.8s to 3.8s and 4.2s to 5.2s respectively. Although this doesn't cover all the data points, it should include an array with an equal number of ratios for all three major peaks individually for the DLC steering input waveform, without the influence of extreme ratios. Finally, the mean of the ratios from each time windows are evaluated, which in turn, the means for those time windows can be computed, giving the final mean ratio that represents the gain of the observer. Following this step will result in a gain of 0.1207 at 40 km/h and 0.2058 at 120 km/h. The estimated yaw rate can be calculated by multiplying this gain with the steering input. Figure 21 shows a comparison between the actual and estimated yaw rate at 40 km/h and 120 km/h.

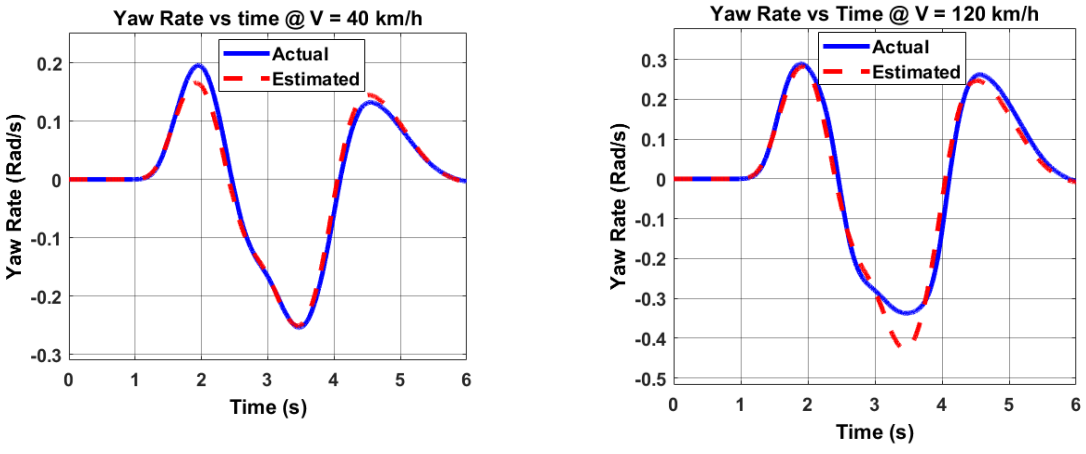

(a) (b)

Figure 21. Yaw rate observer's performances at (a) V = 40 km/h and (b) V = 120 km/h.

The RMS error of the observer is 3.18% at 40 km/h and 2.23% at 120 km/h. For a simple concept, the observer performed well. However, a crucial caveat when using this observer is that this observer is best suited for the same steering input used to derive it since the method of calculating ratios bypasses the nonlinearity of the model instead of reducing the model's complexity. Without building the observer based on the nonlinearity of the vehicle model, the same observer

gain might not perform consistently well if different steering input is used. Besides, the observer is only applicable when the yaw rate and the steering input share the same pattern, like the one used here. If the steering input is a linear line, the yaw rate from the vehicle will be a nonlinear curve, rendering this method inappropriate. In summary, this approach of devising an observer might be faster and more efficient than the conventions, especially if the practitioner wishes to save time developing less critical control system prototypes as a proof of concept. Hence, this paper endorses the adoption of this concept if the user acknowledges its limitations.

RESULTS ANALYSIS USING VARIOUS WIND DISTURBANCE MODEL

This section shall detail all the disturbance tests conducted and discuss on their results. In this study, the usual disturbance test without steering input will be conducted, which is then followed by another one with steering input as the latter experiment isn't covered so often by other scholars.

Wind Disturbance Model

In this research, three different wind profiles (A, B and C) are designed to be used to test the controller's performance in terms of flexibility in coping with different disturbance profile and the amount of disturbance attenuated by the controllers. An additional wind profile D with a much larger magnitude is meant to emulate extreme wind conditions in the real world, and it is used with the nonzero steering disturbance test. All the wind profiles are depicted in Figure 22. These wind profile gives the magnitude of F_{wind} which is presented in Eq. (10), Eq. (15), and Eq. (16).

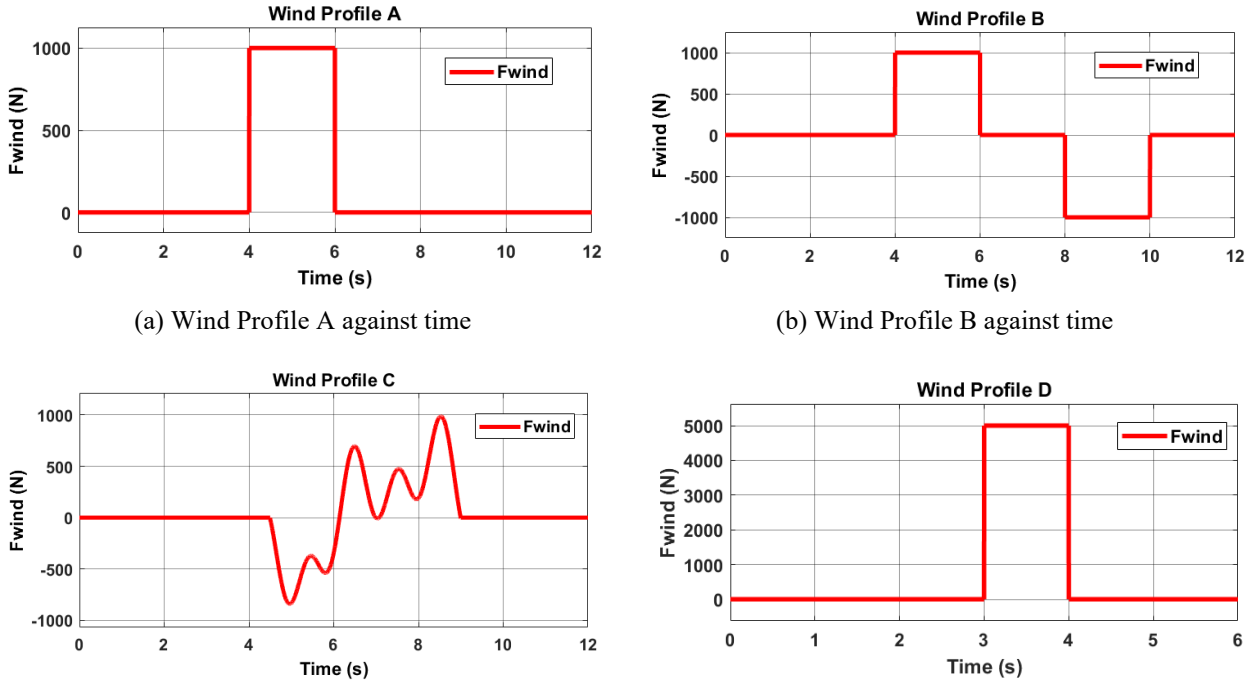

(a) Wind Profile A against time

(b) Wind Profile B against time

(c) Wind Profile C against time

(d) Wind Profile D against time

Figure 22. Wind disturbance profile.

Disturbance Test with Zero Steering Input

The three controllers were tested with two different longitudinal speeds, which are 40 km/h and 120 km/h at zero steering input, and in each case the controllers were tested on wind profiles A, B and C, respectively. For all cases of longitudinal speed, the angle of wind force, φ is kept at 90°. The distance between CoP and CoG, also abbreviated as C is kept constant at a value of 1.016 m, which means the wind force is acting at the same position as the front wheel axle. The choice of CoP allows a large disturbance moment to act on the passenger vehicle. Four outputs – the yaw rate, lateral displacement, sideslip angle and yaw angle will be used to evaluate the performances of each controller. The simulation runs with a Runge-Kutta fixed-step solver with a step size of 0.001 via SIMULINK. The results of the experiment at both vehicle speeds will be discussed together at the end of this subsection.

Figure 23 to Figure 25 shows the results of this disturbance test for each wind profile at V = 40 km/h. Figure 26 to Figure 28 shows the results of this disturbance test for each wind profile at V = 120 km/h. Based on the yaw rate output from Figure 23 to Figure 28, the trend in the amount of yaw disturbance attenuation is the same for each controller for all three wind profiles at both speeds. Hence, only the percentage of attenuation according to wind profile A will be computed, and the results are tabulated in Table 9. The percentage of attenuation is the amount of disturbance rejected by the controllers, which is evaluated using RMS values of the yaw rate output with and without the controller.

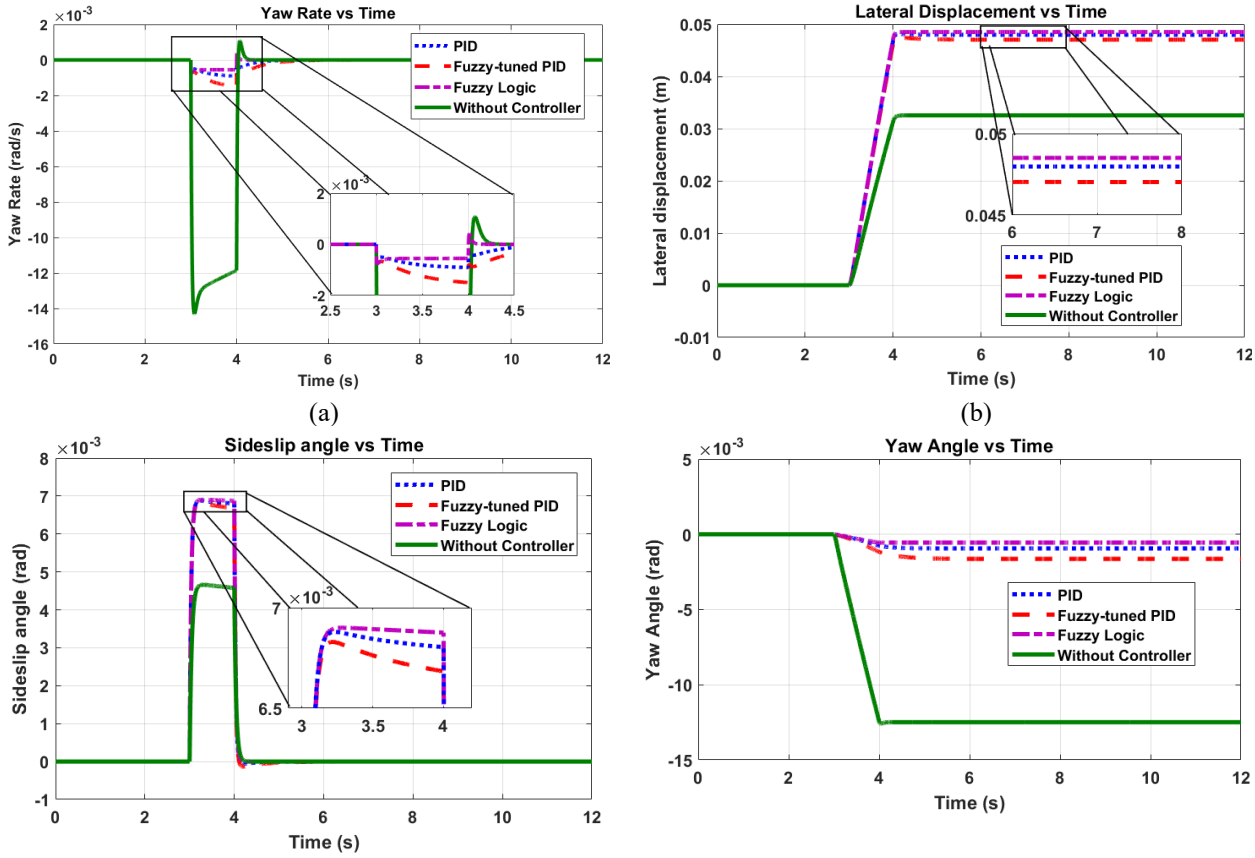

Figure 23. Performance of each controller due to the effect of wind profile A at 40 km/h. (a) Yaw rate vs time, (b) lateral displacement vs time, (c) sideslip angle vs time and (d) yaw angle vs time.

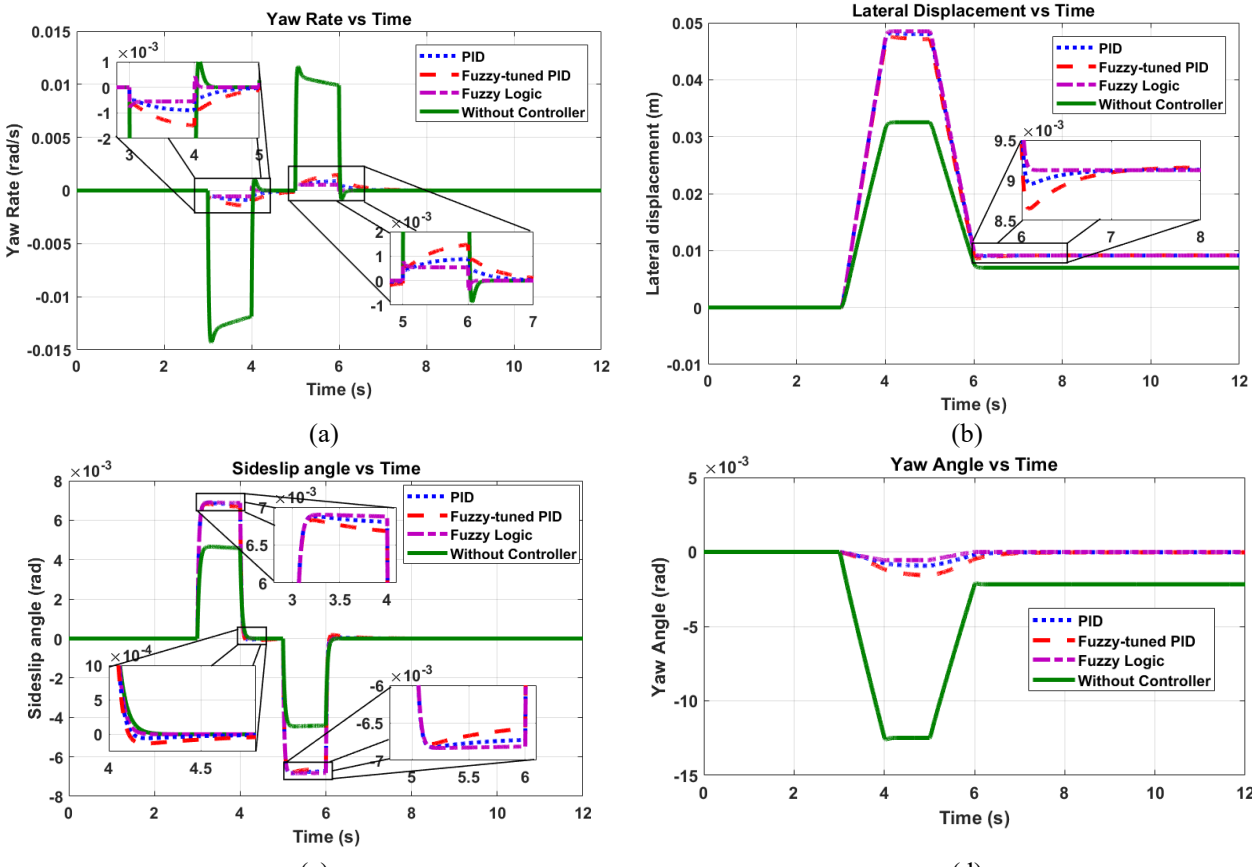

Figure 24. Performance of each controller due to the effect of wind profile B at 40 km/h. (a) Yaw rate vs time, (b) lateral displacement vs time, (c) sideslip angle vs time and (d) yaw angle vs time.

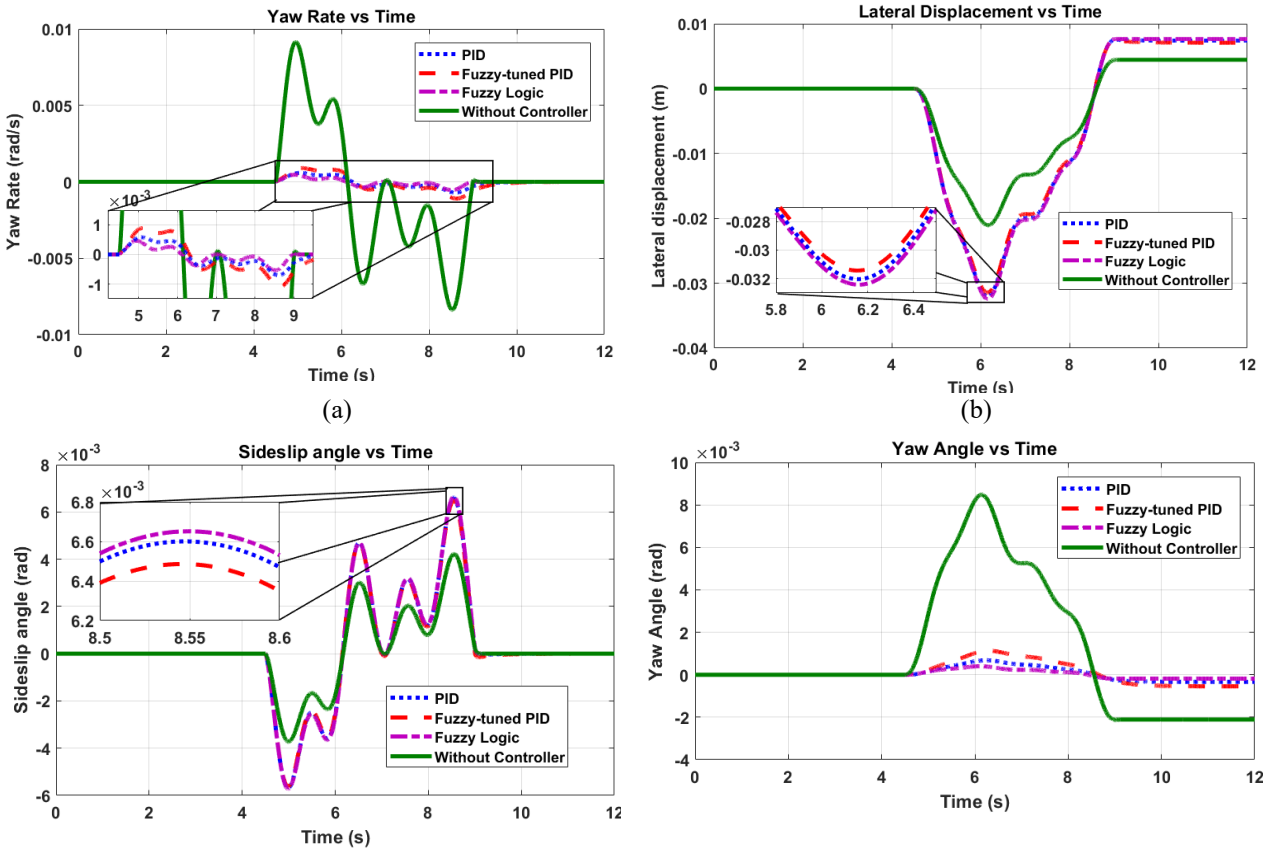

Figure 25. Performance of each controller due to the effect of wind profile C at 40 km/h. (a) Yaw rate vs time (b) Lateral displacement vs time, (c) sideslip angle vs time and (d) yaw angle vs time.

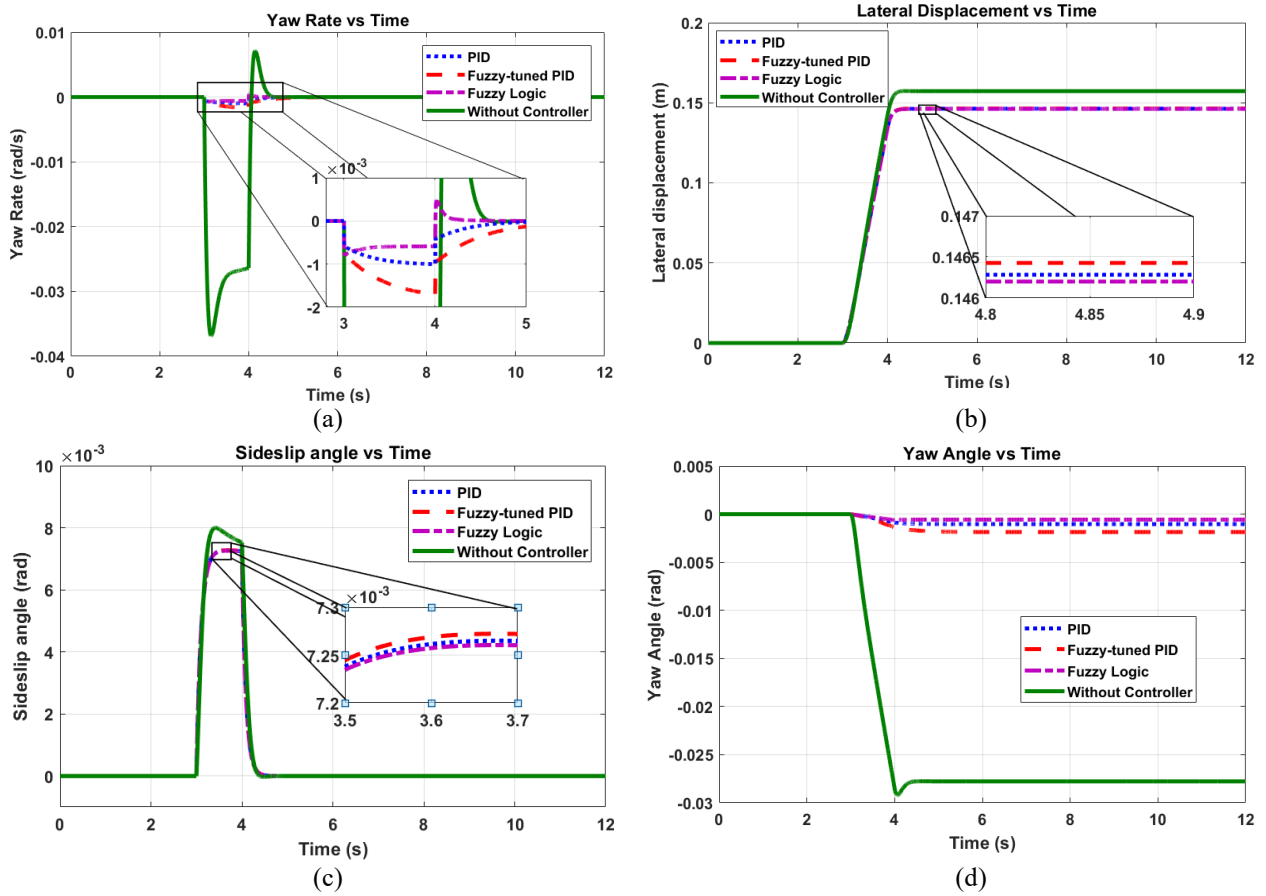

Figure 26. Performance of each controller due to the effect of wind profile A at 120 km/h. (a) Yaw rate vs time, (b) lateral displacement vs time (c) sideslip angle vs time and (d) yaw angle vs time.

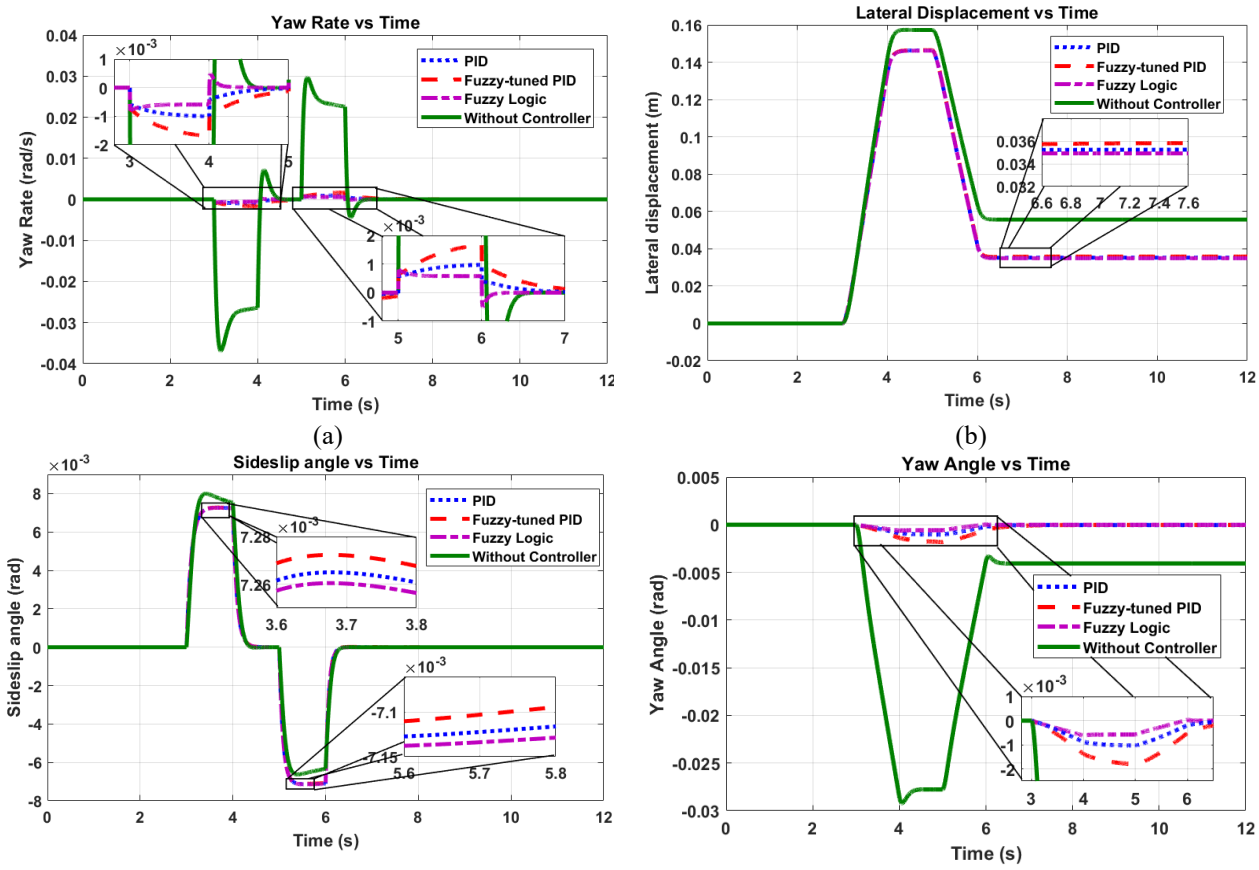

Figure 27. Performance of each controller due to the effect of wind profile B at 120 km/h. (a) Yaw rate vs time, (b) lateral displacement vs time, (c) sideslip angle vs time and (d) yaw angle vs time.

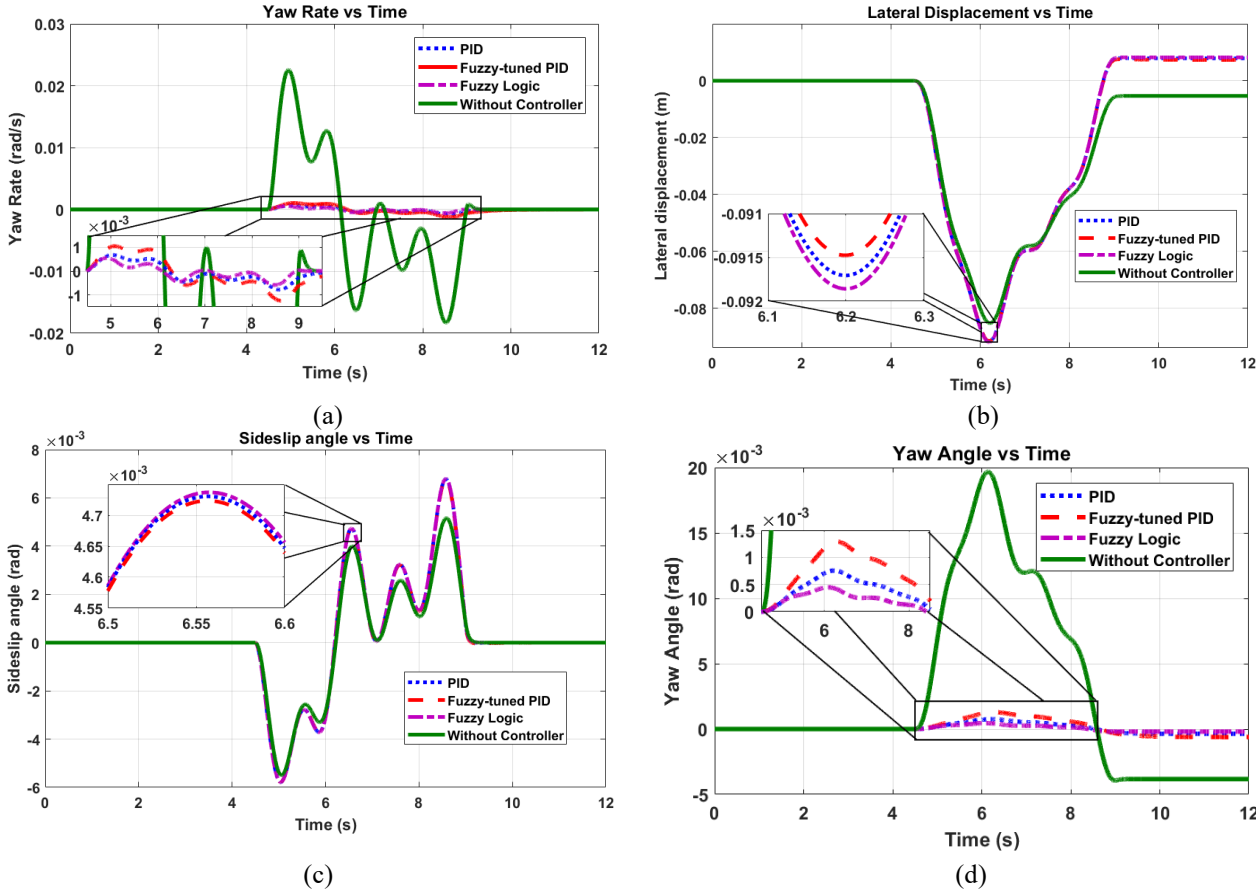

Figure 28. Performance of each controller due to the effect of wind profile C at 120 km/h. (a) Yaw Rate vs time, (b) lateral displacement vs time, (c) sideslip angle vs time and (d) yaw angle vs time.

Table 9. Percentage of attenuation of yaw disturbance for wind profile A at 40 km/h and 120 km/h.

Controllers	Percentage of attenuation (%)		Profiler report execution time (s)
	V = 40 km/h	V = 120 km/h	
PID	93.6	96.9	166.73
Fuzzy-tuned PID	89.7	94.9	277.14
Fuzzy Logic	95.5	97.8	221.98

From Table 9, all three controllers performed equally well. The controllers performed better at 120 km/h because the disturbance at this speed is larger than that at 40 km/h, which leads to a larger difference in RMS values. Even though the performances of all controllers are tight, a few factors could separate the controllers from one another. First, by enabling SIMULINK's profiler report, it returns the computation time of the simulation given in Table 9. This simulation time is exaggerated from the actual value as running the profiler report takes a longer time than without. This proves that Fuzzy-tuned PID is the slowest to compute, which is unsurprisingly due to two controllers constituting it. According to the magnified plot in the yaw rate output in Figure 30 to Figure 35, it is noted that the Fuzzy Logic controller converges the yaw rate to set point (zero) much faster than PID and Fuzzy-tuned PID, to which the latter two exhibit over-damping patterns. Consequently, for the disturbance test without steering input, it can be deduced that Fuzzy Logic outperforms PID and Fuzzy-tuned PID. Controller performances aside, from Figure 23(b)-23(d) to Figure 28(b)-28(d), the values of those outputs didn't return to zero after the disturbance as those variables aren't feedback variables for controller use. In other words, they aren't being corrected by the controllers.

Disturbance Test with Nonzero Steering Input

This disturbance test was further verify the controllers' performances when the driver is steering the vehicle. The settings for this test are similar to the previous, with a few changes as described below:

i. Only wind profile D is used here. This disturbance has a very huge magnitude to emulate extreme conditions.
ii. As the controller shows a similar trend at a vehicle speed of 40 km/h and 120 km/h, only one speed is tested here, which will be 40 km/h as this speed can be realistically applied to the driver when he is steering the vehicle.
iii. The steering input used in this test would be the same DLC steering input used to devise the observer gain. For 40 km/h, the gain is 0.1207.

Besides the slight change in the test settings, the Fuzzy Logic controller needed a retune for this test to ensure the controller was able to correct the disturbance, which it couldn't otherwise. Retuning involves only recalibrating the range for the error, error rate and correction angle. The membership functions for the inputs and output are still similar. The parameters for the PID and Fuzzy-tuned PID are unchanged, however. Figure 29(a) to 29(c) respectively shows the integration of the yaw rate observer with the closed loop system for PID, Fuzzy-tuned PID and Fuzzy Logic controller.

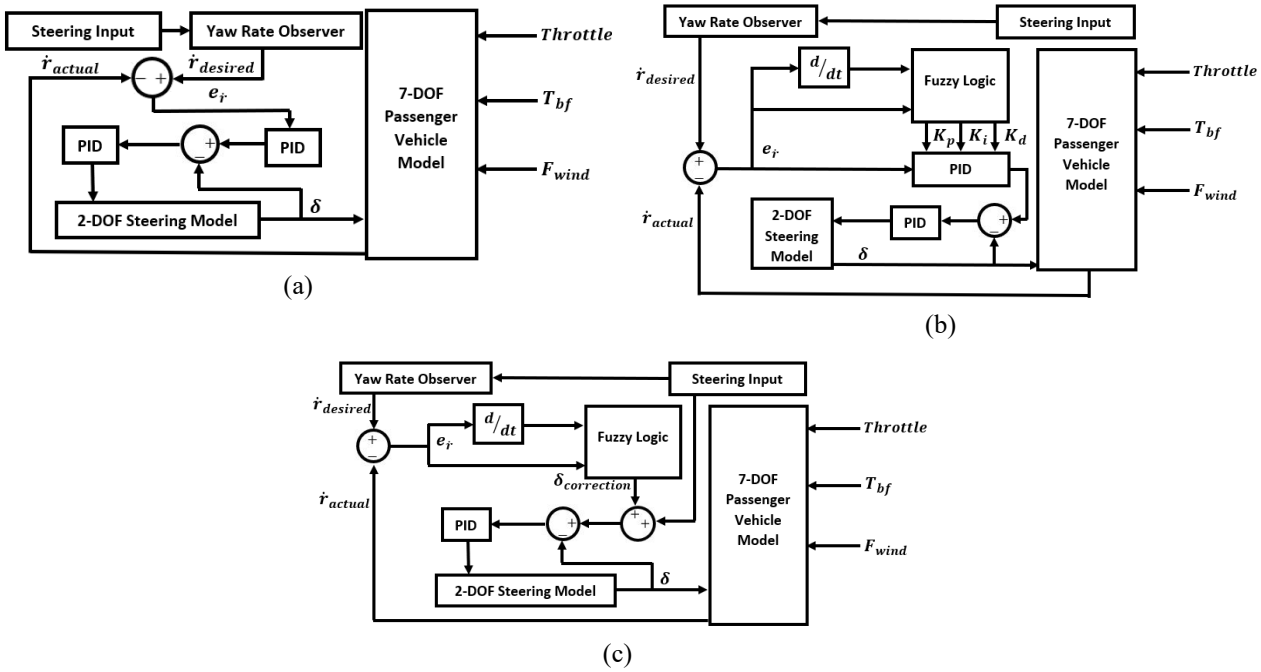

Figure 29. System with (a) PID and yaw rate observer, (b) fuzzy-PID and yaw rate observer and (c) fuzzy logic and yaw rate observer.

As it was discovered from the previous disturbance test that yaw rate was the only output that was corrected by the controller, the yaw rate will be the only output monitored in the current disturbance test. Figure 30(a) to 3(c) represent a yaw rate plot that illustrates the controlled output with the actual yaw rate (desired value) and the uncontrolled output for

PID, Fuzzy-tuned PID and Fuzzy Logic controller, respectively. Figure 31 includes the yaw rate result for each controller to compare their performances directly.

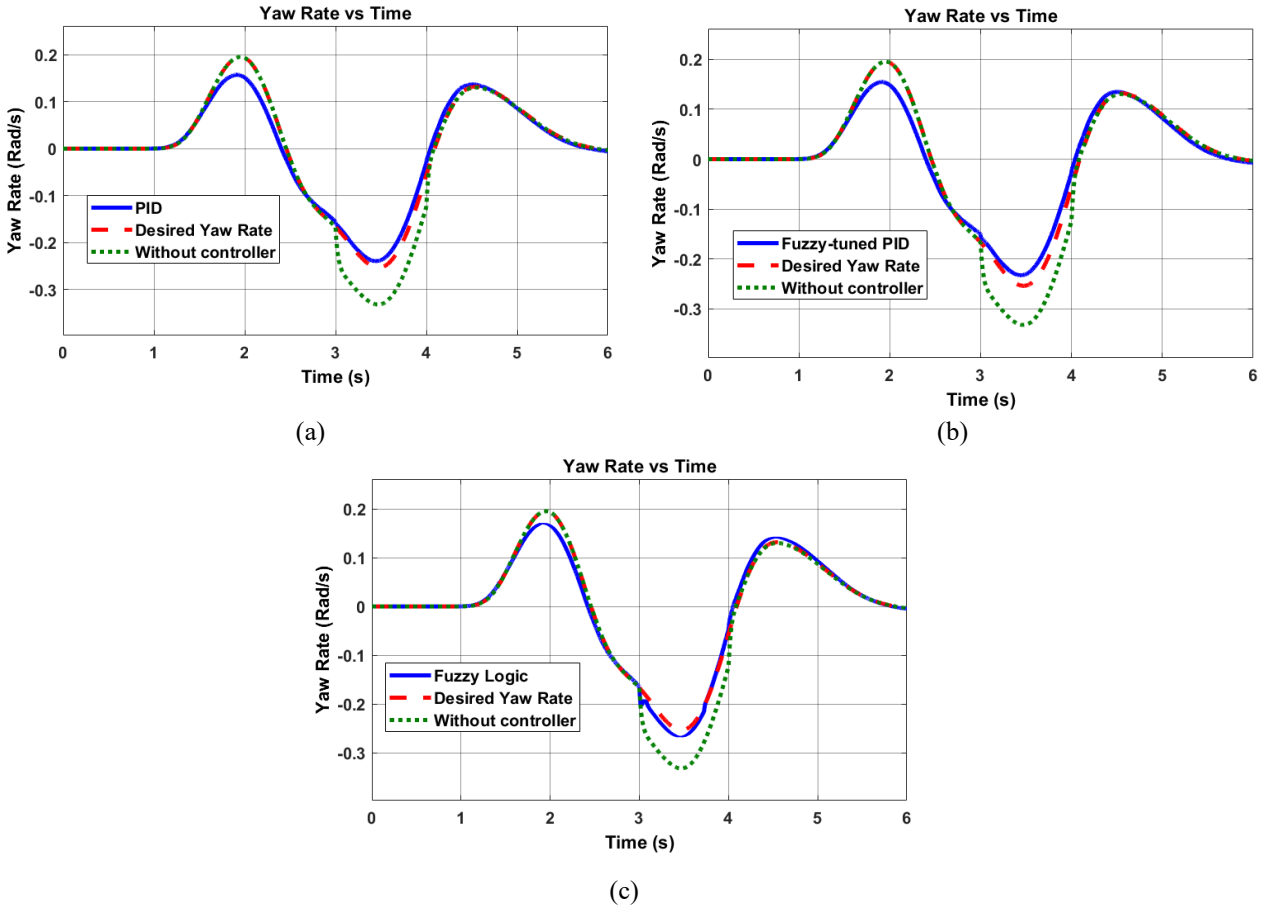

Figure 30. Nonzero steering input disturbance result for (a) PID, (b) fuzzy-tuned PID and (c) fuzzy logic controller.

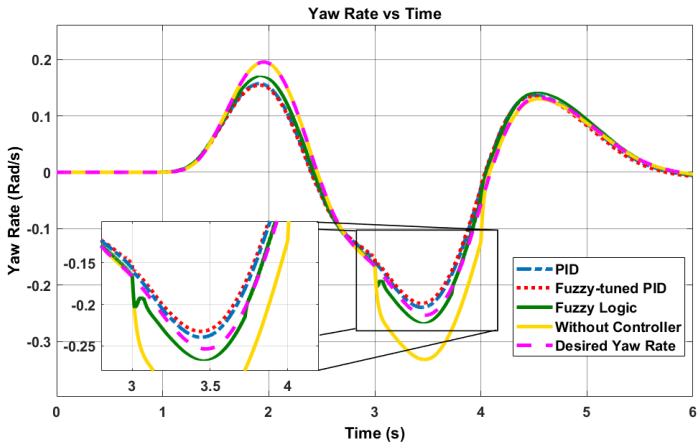

Figure 31. Comparison of performance for all controllers for nonzero steering input disturbance test.

The controllers are judged based on the RMS error in tracking the actual yaw rate (desired value). However, the error of the controller is affected by the error of the observer, which is carried forward into this test. This observer error is noticeable in Figure 30(a) to 30(c), whereby the yaw rate output didn't take after its actual shape before and after the disturbance. To compensate for the observer error, the controllers are scored based on the error in tracking the observer's yaw rate. Both types of tracking errors are tabulated in Table 10.

Table 10. Tracking error for the disturbance test with nonzero steering input.

Controller	Tracking error of yaw rate (%)	
	w.r.t Actual yaw rate	w.r.t observer's yaw rate
PID	7.97	4.95
Fuzzy-tuned PID	10.23	7.28
Fuzzy logic	1.16	4.48

From Table 10, the tracking error with respect to the observer's yaw rate approximates the true error of the controllers because most of the error originates from the disturbance. This also reduces bias in the result, as the tracking error of the fuzzy logic controller increases when the observer error is compensated. This increase in error for the fuzzy logic controller is contributed by the slight inaccuracy in tracking the observer's yaw rate and this inaccuracy would have favoured the fuzzy logic controller in tracking the actual yaw rate. Albeit the fuzzy logic controller was retuned, its performance is on par with the PID controller. If the PID controller is retuned for better gains, it might outperform the fuzzy logic controller. Nevertheless, all controllers performed outstandingly to extreme wind disturbances while simultaneously tracking the desired trajectory of the vehicle.

CONCLUSION

In this paper, a 9-DOF passenger vehicle model was successfully developed and verified by IPG CarMaker data to be used together with the AFWS concept to simulate the vehicle behaviour to lateral wind disturbances. To aid the vehicle's stability, three different controllers, PID, fuzzy-tuned PID and fuzzy logic were developed to dampen the yaw disturbances on the vehicle. The controllers' resiliency and attenuation performances were tested by administering three different wind disturbances to the vehicle without steering intervention and all three controllers showed almost identical performances, that is, removing at least 90% of the disturbances from the yaw rate at two different vehicle speed. However, fuzzy-tuned PID was the slowest in computation. Fuzzy logic exhibited a critical damping pattern in the yaw rate output, which is important to ensure the vehicle is free from the aftermath immediately. The controllers were further verified for their performances through a disturbance test using a stronger wind disturbance and with steering input. Before that, a yaw rate observer without state space modelling and black box algorithm was devised using a simple concept and successfully estimated the actual yaw rate with an error of less than 4% at speeds of 40 km/h and 120 km/h. Using this observer as the reference yaw rate and also compensating for the observer's error, the three controllers had a tracking error of less than 8%, with most of the disturbance rejected. Since fuzzy logic had a slightly lower error, it was rendered as the best performing controller out of the trio in this experiment.

ACKNOWLEDGEMENT

This work is part of the research project entitled "Vehicle-in-the-loop Safety Testing Platform for Autonomous Vehicle using Malaysian Road and Traffic Environment". This research is fully supported by Yayasan Tun Ismail Mohamed Ali Berdaftar (YTI) under Permodalan Nasional Berhad and the grant is led by Assistant Professor Dr. Vimal Rau Aparow. I also would like to thank University of Nottingham Malaysia for continuous support in conducting research in this area.

REFERENCES

[1] B. Aalizadeh, "A neurofuzzy controller for active front steering system of vehicle under road friction uncertainties," *Trans. Inst. Meas. Control*, vol.41, pp.1057-1067, 2019, doi: 10.1177/0142331218780220.

[2] X. Diao, Y. Jin, L. Ma, S. Ding and H. Jiang, "Composite active front steering controller design for vehicle system." *IEEE Access*, vol. 5, pp.6697-6706, 2017.

[3] N. Sang, and C. Lele, "Design of an active front steering system for a vehicle using an active disturbance rejection control method." *Science Progress*, Vol. 103, No. 1, 0036850419883565, 2020.

[4] Y. Wu, L. Wang, J. Zhang, and F. Li, "Robust vehicle yaw stability controlby active front steering with active disturbance rejection controller." Proceedings of the Institution of Mechanical Engineers, *Part I: Journal of Systems and Control Engineering*, vol. 233, no. 9, pp. 1127-1135, 2019.

[5] W. Zhao, Z. Han and Y. Li. "Displacement and force coupling control design for automotive active front steering system." *Mech. Syst. Signal Process.*, vol. 106, pp. 76-93, 2018.

[6] S. A. Saruchi, Z. Hairi., N. Zulkarnain, and M. H. Mohammed, "Composite nonlinear feedback with disturbance observer for active front steering," *Indones. J. Electr. Eng. Comput. Sci.*, vol. 7, no. 2, pp. 434-441, 2017.

[7] K. Hudha, M. H. Zakaria, and N. Tamaldin, "Hardware in the loop simulation of active front wheel steering control for yaw disturbance rejection," *Int. J. Veh. Saf.*, vol.5, no.4, pp. 356-373, 2011, doi: 10.1504/IJVS.2011.045776.

[8] X. Ma, P. K. Wong, J. Zhao, and Z. Xie, "Cornering stability control for vehicles with active front steering system using T-S fuzzy based sliding mode control strategy," *Mech. Syst. Signal Process.*, vol. 125, pp. 347-364, 2019, doi: 10.1016/j.ymssp.2018.05.059.

[9] B. Aalizadeh and A. Asnafi, "Fuzzy versus neuro-fuzzy identification of active front steering of a vehicle on slippery roads," *Int. J. Automot. Mech. Eng.*, vol. 16, no. 1, pp. 6078-6089, 2019, doi: 10.15282/ijame.16.1.2019.1.0463.

[10] A. Saikia and C. Mahanta, "Vehicle stability enhancement using sliding mode based active front steering and direct yaw moment control," In 2017 Indian Control Conference, ICC 2017 - Proceedings, 2017, pp. 378-384 doi: 10.1109/INDIANCC.2017.7846504

[11] V. R. Aparow, K. Hudha, Z. A. Kadir, N.H. Amer, S. Abdullah and M. M. M.Ahmad. "Identification of an optimum control algorithm to reject unwanted yaw effect on wheeled armored vehicle due to the recoil force," *Adv. Mech. Eng.*, Vol.9, No. 1, pp.1-16, 2016, 1687814016683350.

[12] M. Mansor *et al.*, "Modelling and optimization of active front wheel steering system control for armoured vehicle for firing disturbance rejection," *Int. J. Veh. Auton. Syst.*, vol. 13, no. 4, pp.306-329, 2017.

[13] V. R. Aparow, K. Hudha, M. M. H. M. Ahmad and S. Abdullah, "Development of estimated disturbance rejection feedback for an armoured vehicle using active front wheel steering." *Int. J. Adv. Mechatron. Syst.*, vol. 7, no. 3, pp.134-143, 2017.

[14] Z. A. Kadir *et al.*, "Modeling and implementation of yaw disturbance rejection control for an instrumented armoured vehicle to minimize the effect of unwanted recoil force," In 2018 57th Annual Conference of the Society of Instrument and Control Engineers of Japan (SICE), 2017, pp. 1538-1543.

[15] V. R. Aparow *et al.*, "System configuration of instrumented half-scaled armoured vehicle to enhance handling performance due to lateral firing impact," *Int. J. Adv. Mechatron. Syst.*, vol. 9, no. 1, pp.21-29, 2021.

[16] V. R. Aparow *et al.*, "Firing-on-the-move stability system for armoured vehicle: design and optimization of disturbance rejection control to reject recoil force," *Int. J. Heavy Veh. Syst.*, vol. 26, no. 5, pp.599-627, 2019.

[17] H. Zhang and J. Wang, "Vehicle lateral dynamics control through afs/dyc and robust gain-scheduling approach," *IEEE Trans. Veh. Technol.*, vol. 65, no. 1, pp. 489–494, 2016, doi: 10.1109/TVT.2015.2391184.

[18] B. Li, S. Rakheja, and Y. Feng, "Enhancement of vehicle stability through integration of direct yaw moment and active rear steering," *Proc. Inst. Mech. Eng. Part D J. Automob. Eng.*, vol. 230, no. 6, pp. 830-840, 2016, doi: 10.1177/0954407015596255.

[19] V. R. Aparow, K. Hudha, MMHM Ahmad and H. Jamaluddin, "Development and Verification of a 9-Dof Armored Vehicle Model in the Lateral and Longitudinal Directions," *Jurnal Teknologi*, vol. 78, no. 6, 2016.

[20] F. Ahmad, K. Hudha, S. A. Mazlan, H. Jamaluddin, V. R. Aparow and M. M. Yunos, "Simulation and experimental investigation of vehicle braking system employing a fixed caliper based electronic wedge brake," *simulation*, vol. 94, no. 4, pp.327-340, 2018.

[21] V. R. Aparow *et al.*, "Model-in-the-loop simulation of electronically controlled pitman arm steering mechanism for armored vehicle," In 2016 SICE International Symposium on Control Systems (ISCS), 2016, pp. 1-6.

[22] H. R. Ramesh and D. S. R. Shankapal, "Modeling, simulation and implementation of a proportional-derivative controlled column-type EPS," I*nt. J. Enhanc. Res. Sci. Technol. Eng*., vol. 2, no. 9, pp. 10–19, 2013.